

IMPACT OF PLANT CO₂ PHYSIOLOGICAL FORCING ON EXTREME HEAT AND
HUMIDITY EVENTS

by

ASHLEY CORNISH

(Under the Direction of Gabriel Kooperman)

ABSTRACT

21st Century projections of climate change from Earth system models demonstrate increasing global temperatures in response to rising levels of greenhouse gas concentrations, most notably carbon dioxide (CO₂). These warming temperatures are associated with greater heat index. In addition to radiative forcing, recent work has shown that biogeochemical plant physiological forcing also contributes to changes in these extreme heat events through changing evapotranspiration. Using the Community Earth System Model Versions 1 and 2 (CESM1 and CESM2), we analyze the radiative, physiological, and combined impacts of a 1% per year increase to 4xCO₂ to find increases and/or decreases in temperature, moisture, and combined temperature-moisture indices. We further isolate the roles of changes in leaf area index (LAI) and stomatal resistance as represented in CESM1 vs. CESM2. Additionally, we determine the whether or not hourly temporal scale temperature and relative humidity is necessary for the calculation of the heat index.

INDEX WORDS: Earth System Modeling, Climate, Extreme Heat, Plant Physiology Impacts

IMPACT OF PLANT CO₂ PHYSIOLOGICAL FORCING ON EXTREME HEAT AND
HUMIDITY EVENTS

by

ASHLEY CORNISH

Bachelor of Science in Meteorology, Rutgers University, 2020

A Thesis Submitted to the Graduate Faculty of The University of Georgia in Partial Fulfillment
of the Requirements for the Degree

MASTER OF SCIENCE

ATHENS, GEORGIA

2022

© 2022

Ashley Cornish

All Rights Reserved

IMPACT OF PLANT CO₂ PHYSIOLOGICAL FORCING ON EXTREME HEAT AND
HUMIDITY EVENTS

by

ASHLEY CORNISH

Major Professor: Gabriel Kooperman
Committee: Andrew Grundstein
Christopher Skinner

Electronic Version Approved:

Ron Walcott
Vice Provost for Graduate Education and Dean of the Graduate School
The University of Georgia
August 2022

DEDICATION

To my family who has supported me my whole life; and the friends that became family here in Athens.

ACKNOWLEDGEMENTS

I acknowledge support from the U.S. Department of Energy Regional and Global Model Analysis Program (DE-SC0019459 and DE-SC0021209).

TABLE OF CONTENTS

	Page
ACKNOWLEDGEMENTS	v
LIST OF FIGURES	viii
CHAPTER	
1 INTRODUCTION	1
Research Questions	4
2 LITERATURE REVIEW	5
Warming Global Temperatures	5
Previous Studies Including Physiological Effects	5
Evapotranspiration and Extreme Heat	7
Stomatal Conductance	8
Plant Growth and Leaf Area	8
Temperature and Moisture Indices	10
3 METHODS	12
Community Earth System Model (CESM)	12
Community Atmosphere Model (CAM)	13
Community Land Model (CLM)	14
Coupled Model Intercomparison Project DECK and C4MIP Experiments	15
Temperature and Heat Index Extremes	17

4	RESULTS.....	18
	PART 1: Determining the necessity of hourly temperature and humidity data to calculate the heat index and its response to climate change.....	18
	PART 2: Changes in the Heat Index and its Radiative and Plant Physiological Components under Increased CO ₂ in the Community Earth System Model Versions 1 and 2	32
	PART 3: Disentangling the competing influences of plant physiological forcing on heat and atmospheric moisture changes	51
5	DISCUSSION.....	59
6	CONCLUSION	60
	REFERENCES	62

LIST OF FIGURES

	Page
Figure 1: Schematic Representing the role increased CO ₂ on plants and extreme heat.....	10
Figure 2: Classification of Heat Index Values	11
Figure 3: Schematic of the CESM2 component models	13
Figure 4: Graphical Representation of the C4MIP simulations	16
Figure 5: Differences of Heat Index Calculation Methods.....	19
Figure 6: Diurnal Cycles in the Sahel Region	21
Figure 7: Diurnal Cycles in Central Africa	21
Figure 8: Annual Distributions in the Sahel	24
Figure 9: Annual Distributions in Central Africa.....	24
Figure 10: Distributions of Hourly and Daily HI at Finer Bin Spacing	25
Figure 11: Differences of Heat Index Calculation Methods of the Change	27
Figure 12: Annual Distributions of the Change in the Sahel.....	28
Figure 13: Annual Distributions of the Change in Central Africa	28
Figure 14: Averages and Difference of Days in NWS Categories	29
Figure 15: Change in the Number of Days in a Year Classified as Caution or Danger	30
Figure 16: Difference of Days in NWS Categories of the Change	31
Figure 17: Mean Heat Index Change.....	33
Figure 18: 99 th Percentile Heat Index Change.....	35
Figure 19: Combined NWS Category Changes CESM1	38

Figure 20: Combined NWS Category Changes CESM2.....	39
Figure 21: Mean Temperature Change.....	40
Figure 22: 99 th Percentile Temperature Change.....	42
Figure 23: Differences of HI and Temperature	44
Figure 24: 99 th Percentile HI and Temperature Difference	45
Figure 25: Mean Relative Humidity Change.....	47
Figure 26: Mean Specific Humidity Change.....	49
Figure 27: Mean Leaf Area Index Change	52
Figure 28: Mean Evapotranspiration Change.....	53
Figure 29: Mean Canopy Transpiration Change	54
Figure 30: Mean Canopy Evaporation Change	56
Figure 31: Mean Ground Evaporation Change	57

CHAPTER 1

INTRODUCTION

By the end of the 21st century, carbon dioxide emissions rates are projected to reach over 100GtCO₂ per year under the highest emission scenario (i.e., economy heavily reliant on fossil fuels). With these rates, total CO₂ concentrations are projected to reach over 1100 ppm. (Arias et al., 2021) Additionally, under this scenario, global temperatures are likely to increase between 3.3°C to 5.7°C, compared to the 1850-1900 global average surface temperature, with majority of this warming being driven by increasing CO₂ (IPCC, 2021). In addition to rises in average temperatures, increases in extreme events, such as heat waves, are also projected. In recent years, heat extremes have increased in intensity, duration, and frequency (Perkins-Kirkpatrick & Lewis, 2020), and model projections are showing these trends will continue (Arias et al., 2021; Donat et al., 2018; Kala et al., 2016; Skinner et al., 2018; Ukkola et al., 2018). These changes in temperature impact natural ecosystems and society, including agriculture, industry, and human health; with grave implications for human mortality. Such an example is the 44-day heatwave in the Russian Federation in 2015 which lead to 56,000 deaths (WHO, 2018). Zhao et al., (2021) found that in a study from the year 2000-2019, there were approximately 490,529 deaths per year related to non-optimal heat on a global scale. Majority of these deaths were seen Eastern Europe. A substantial portion of heat-related deaths can be attributed to climate change as seen in Vicedo-Cabrera et al., (2021).

Exposure to extreme heat compromises the body's ability to regulate temperature and can result in heat stress, leading to a variety of heat related illnesses including heat cramp and heat

exhaustion (Grundstein et al., 2018). More vulnerable populations such as children, the elderly, athletes, the poor, displaced, homeless, as well as outdoor workers will feel the impacts on a more substantial scale (WHO, 2018). These impacts will further be exacerbated as nighttime temperature warm, inhibiting the body's ability to cool off at night. It is thus critical to understand how the regional patterns of extreme temperature changes coincide with these vulnerable populations, and in particular the physical processes that may influence these changes over the 21st century.

Furthermore, increased temperatures are not the only factor that determines health implications for humans. To investigate the direct impacts, a parameter that also includes atmospheric moisture content is essential to consider. One example is the heat index (HI) (Lee & Brenner, 2015; Rothfus, 1990), which combines relative humidity (RH) and temperature (T) to better emphasize the stress felt by humans under extreme heat events. Humans are adept to cool down by sweating, which utilizes heat energy from our bodies to evaporate sweat off the skin surface. In cases of high RH, heat dissipation from the skin surface is reduced due to the reduced evaporative capacity of the environment. The reduction of dissipation leads to a decrease in sweat evaporation efficiency, and increased temperature at the skin's surface. The higher skin temperature increases skin blood flow and circulatory strain, leading to heat-related illnesses such as heat stress and heat stroke (Che Muhamed et al., 2016).

As global temperatures increase, high HI is projected to become more of a threat, as days with dangerously high levels are projected to become more frequent (Koteswara Rao et al, 2020). On one hand, higher temperature can lead to higher specific humidity, based on the Clausius-Clapeyron relationship; but higher temperature also reduces relative humidity. Globally, relative

humidity remains relatively constant, but regional changes, particularly over land, are more complicated and depend on soil moisture and land-surface conditions.

While the majority of the temperature increase projected in the future results from an enhanced greenhouse effect, an important and relatively unexplored control on atmospheric moisture and temperature over land is the throttling of evapotranspiration via plant physiological responses to higher CO₂. Previous studies (Skinner et al., 2018; Kala et al., 2016) have demonstrated the effect of plant CO₂ physiological forcing on heat extremes, particularly through a reduction in stomatal conductance (i.e., the closing or opening of the stomata, the pores on the plants leaves and stem) when atmospheric CO₂ concentrations rise. These studies focus on heat waves and/or heat extremes, which are an important indicator of the ways environments will change under a warming climate; but have not included a direct assessment of the moisture component. For the analysis presented here, I quantify how plant CO₂ physiological forcing (i.e., reductions in stomatal conductance, changes in leaf area, etc.) may increase or decrease surface temperature and relative humidity, and thus influence changes in the HI in response to rising CO₂ using a controlled set of Earth system model experiments. By focusing on HI, a parameter that emphasizes the heat stress felt by humans in more humid conditions, I investigate the competing effects of reduced evapotranspiration on temperature and humidity.

Research Questions

1. Is there a necessity for hourly temperature and humidity data to calculate the heat index and its response to climate change?
2. What is the contribution of plant physiological forcing under increased CO₂ to changing atmospheric moisture, temperature, and heat index?
3. What are the competing influences of plant physiological forcing on heat and atmospheric moisture changes?

CHAPTER 2

LITERATURE REVIEW

Warming global temperatures

With rising greenhouse gas concentrations and associated increasing global average temperatures, comes changes to frequency, intensity and statistics of heat extremes on regional, spatial, and seasonal temporal scales (IPCC, 2021). Under a 2.0°C increase in global average temperature, there are robust projected changes in the spatial patterns of the hottest days of the year. Areas of Saharan and southern Africa, portions of the Amazon, Middle East, and the Eastern United States are projected to experience a ~4.0°C average increase to the hottest days. Temperature increases are even more pronounced in the change to the average temperature of the coldest nights of the year. The most intense increases are found in the polar regions, where in the Northern Hemisphere regions of eastern Russia, nighttime temperatures are expected to rise by around 10.0°C (Hoegh-Gulberg et al., 2018).

Previous Studies Including Physiological Effects

Plant-physiological effects are the ways that changes to plant functions influence other parts of the global climate system. These can include processes such as increased leaf area, decreasing albedo, or decreased transpiration decreasing atmospheric moisture. The contributions of plant-physiological effects to changes in climate, including extreme events, have recently gained attention in a number of areas, such as: temperature (Skinner et al., 2018), drought (Swann et al., 2016), runoff (Kooperman et al., 2018), and flooding (Fowler et al., 2019). These studies highlight the key roles that plants play in both water and energy cycles by

assessing CO₂-only simulations that separate the contributions of physiological and radiative (greenhouse) effects (Jones et al., 2016). These include a pre-industrial simulation and three other simulations with a 1% increase in CO₂ concentration per year over 140 years, an increase from 285 ppm to 1140 ppm. The three simulations were (1) both radiative and physiological components experienced increased CO₂ levels; (2) a radiative simulation in which physiology was kept at pre-industrial levels; (3) and a physiological simulation in which radiation was kept at pre-industrial levels. (Jones et al., 2016). This framework will be described in further detail in the Methods section.

Skinner et. al (2018) used this experiment design to assess changes in heat extremes under full, radiative, and physiological simulations. The results showed that when CO₂ concentrations were increased in the Coupled Model Intercomparison Project Phase 5 (CMIP5) models, the leaf area index (LAI) increased, but transpiration declined. The highest amounts of LAI increase were found in the forested regions of the tropics and the mid-latitudes. Despite this, most models exhibited decreases in transpiration over the 140-year simulation due to a larger reduction in stomatal conductance. To investigate drivers of this change and its influence on temperature, the authors compared the simulations separating the radiative and the physiological effects. A summary their results highlighted the probability that out of 120 heatwave days, 100 could be attributed to radiative effects and 40 to physiological effects. Along with this, the mean maximum summer daily temperatures increased by more than 2°C in response to CO₂ vegetation forcing alone in many regions.

Another study done by Kala et al., (2016) conducts an analysis to determine the influence of changing evapotranspiration on heat waves and extreme heat events in Boreal summers in northern Eurasia. They simulate these changes using the “business as usual” emission scenario,

for the period 2019-2099. Through this analysis, they determined there was a 4-5°C increase in the warmest day of the year over areas of western Europe.

Evapotranspiration and Extreme Heat

Changes in surface temperature are often associated with changes to the ratio of latent and sensible heating, in addition to radiative components of the near-surface energy balance. When the ground is mostly saturated, much of the available energy is converted to latent heat, through evaporation, rather than warming the land and air temperature. When there is less moisture available to be evaporated, more of this energy goes to warm the land and increase sensible heating, which warms the overlying atmosphere. The land surface contributes to atmospheric moisture through ground evaporation, canopy evaporation (water collected on the surfaces of leaves), and canopy transpiration, the combination of which is the total evapotranspiration (ET) (Kala et al., 2016) The relation between ET rates and extreme heat events have been studied in recent years, through modeling and observational data. Ukkola et al. (2018) compared CMIP5 model data to observations of temperature and ET rates to test the correlation and evaluate model biases. Through their analysis they found that there was a strong correlation between decreasing ET flux and maximum temperatures for dry climates in observation data. There was agreement between observational and model output data, but only for regions over in the transitional wet to dry regions of Europe and North America (Ukkola et al., 2018). This was in part due to findings that show the land surface models may be overestimating heat extremes over wet and dry regions.

The same regions of Europe and North America were also highlighted in Donat et al. (2018), where there was a strong negative correlation in standardized precipitation index (a metric used to demonstrate the amount of moisture stored in the land surface) and future regional

amplification of the hottest day of the year. However, it is worth noting that metrics based on precipitation changes do not fully account for the influence of vegetation-related processes on ET.

Stomatal Conductance

Plants exert a strong control on total ET through canopy transpiration, which is the largest component of evaporation for many land regions (Kirschbaum & McMillan, 2018). The driving force behind canopy transpiration is the stomata, the pores found on the leaves and stems of plants that allow for gas exchanges between the plants and surrounding environment. To varying degrees, plants seek to optimize how much CO₂ is taken in via stomata for photosynthesis, while losing as little water vapor through the open pores. Under higher atmospheric CO₂ outside the leaf, plants are able to take in as much or more CO₂ with the stomata open less, allowing for less water loss. This statement was proven, when under an increased ambient CO₂ experiment, water use of plants declined (Walker et al., 2014). The extent of closing and opening of the stomata is known as stomatal conductance. The lower stomatal conductance has been shown to reduce the amount of water lost to the environment through decreased transpiration, effecting temperature (Skinner et al., 2018; Kala et al., 2016), precipitation (Kooperman et al., 2018), and other aspects of the climate system. This decrease in ET can reduce latent heating, increasing sensible heating, and warming the environment (Figure 1).

Plant Growth and Leaf Area

CO₂ influences the biological components of the climate system by increasing carbon fixation rates by plants. Increased CO₂ can lead to the enhancement of biomass production, through CO₂ fertilization (Medlyn et al., 2011). In addition to reducing stomatal conductance,

higher CO₂ can have a competing effect on decreased transpiration by increasing plant growth and leaf area (Figure 1). This would increase canopy evaporation, canceling out some of the decrease in canopy transpiration, as well as decrease the surface albedo (more shortwave energy absorbed). Decreased albedo causes more absorption of shortwave radiation in turn increasing outgoing longwave radiation from Earth's surface. Modeling LAI can be difficult, for it depends on a number of environmental factors each with complex relationships. Ewert (2004) shows an increase in LAI by 10-30% when ground surface CO₂ is increased. A 2013 study by Mahowald et al. (2015) tested the accuracy of the model in representing changing rates of LAI. Through their analysis they found that over a large portion of earth, there is an increase in mean LAI, except in regions where there is predicted mean decrease in precipitation.

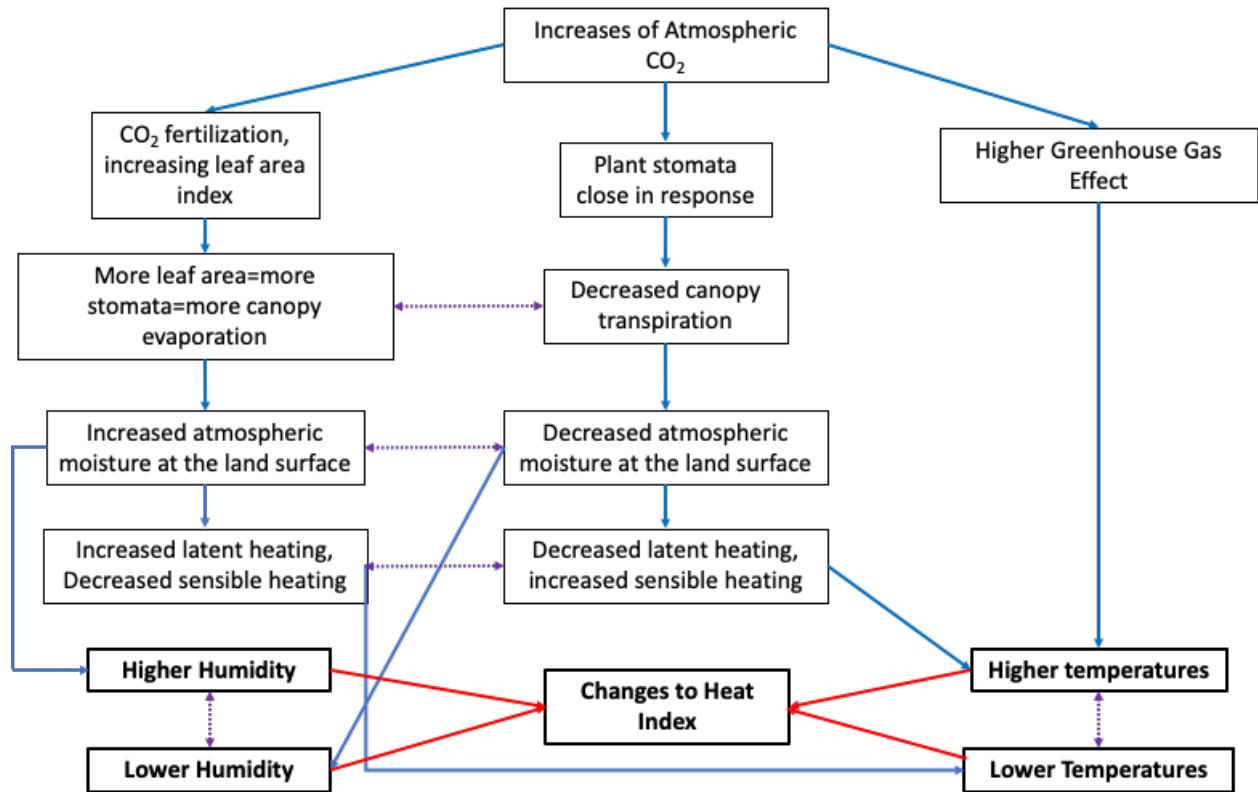


Figure 1: Schematic Representing the role increased CO₂ on plants and extreme heat parameters.

Blue lines represent standard processes, red represent drivers to changing heat index, purple dotted lines represent results with inverse, competing effects.

Temperature and Moisture Indices

While increasing surface temperature is the major driver of amplified heat extremes, it does not capture the full effect of human impacts. Heat index (HI) is a parameter that has been derived to include temperature and humidity together to better demonstrate heat stress. A variety of other indices have been derived for a similar purpose (e.g., temperature humidity index (Segnalini et al., 2013) or the humidex (Masterson and Richardson, 1979), which includes vapor pressure rather than relative humidity. Others have also incorporated influences of wind speed and incoming solar radiation (e.g., Wet Bulb Globe Temperature (Alessi & DeGaetano, 2020)). A study conducted by Lee & Brenner (2015) looked at ERA-Interim gridded reanalysis data to

investigate changes in HI. Between the years 1979 and 2013, they found most regions displaying an increase in heat index, with the notable exceptions of Eurasia and Alaska, which showed decreases in their winter. This raises an important question about the relationship between the diurnal cycles of temperature and humidity, and how non-linearities may influence the calculation of HI from data with limited temporal resolution (often a challenge for available climate data). Bernhardt et al. (2018) and Brockhaus et al. (2008) both note that the diurnal cycle, and the way it is averaged, has an impact on the calculations of averaged daily temperature. This is discussed for a variety of temperature-humidity indices in Buzan et al. (2015) as well, who note the benefit of sub-daily scale data for the calculation of these metrics. This will be further investigated in Part 1 of Results.

Of note, the exact numerical definition of extreme heat when the National Weather Service (NWS) issues heat advisories, excessive heat warnings, and excessive heat watches can differ by region due to the various climatologies of the country. However, the NWS has defined a standard set of categories for heat index and corresponding health risks, broken down in Figure 2. These categories correspond to the likelihood of heat disorders with strenuous activity or prolonged exposure to these high HI values.

Classification	Heat Index	Effect on the body
Caution	80°F - 90°F	Fatigue possible with prolonged exposure and/or physical activity
Extreme Caution	90°F - 103°F	Heat stroke, heat cramps, or heat exhaustion possible with prolonged exposure and/or physical activity
Danger	103°F - 124°F	Heat cramps or heat exhaustion likely, and heat stroke possible with prolonged exposure and/or physical activity
Extreme Danger	125°F or higher	Heat stroke highly likely

Figure 2: Classification of Heat Index Values (Source: NOAA, 2019)

CHAPTER 3

METHODS

In this study, I investigate the processes that contribute to changes in the heat index in response to rising CO₂ using a controlled set of simulations from the Community Earth System Model (CESM). These simulations separate out the effects due to the greenhouse effect (radiation) and plant effect (physiology). The following sections describe CESM, the relevant processes in atmosphere and land components of the model, the experiment simulations, and analysis methodology.

Community Earth System Model (CESM)

This analysis is conducted using the National Center for Atmospheric Research's (NCAR) Community Earth System Models Version 1 (CESM), which was used as part of the Coupled Model Intercomparison Project Phase 5 (CMIP5); and Version 2 (CESM2), which was used as part of CMIP6. CESM1/2 is a fully coupled earth system model (ESM) that includes land (including land biogeochemistry), river runoff, surface waves, ocean (including marine biogeochemistry), land ice, and sea ice components. The different states and fluxes of the various component models are exchanged via a coupler, the Common Infrastructure for Modeling the Earth (CIME5) (Danabasoglu et al., 2020) (Figure 3). In particular, the land-atmosphere coupling includes two-way fluxes of energy and water. The warming of the atmosphere warms the ground, and vice versa. The transpiration from the plant canopy adds moisture to the air. These are just some of the standard earth system processes that benefit from such a coupler.

Research into the climate sensitivities of both versions of CESM show that the climate sensitivity of CESM2 is approximately 1.5K warmer than that of CESM1 (Bacmeister et al., 2020). This could signify that any research conducted into temperature changes within CESM2 would likely be higher than the equivalent in CESM1.

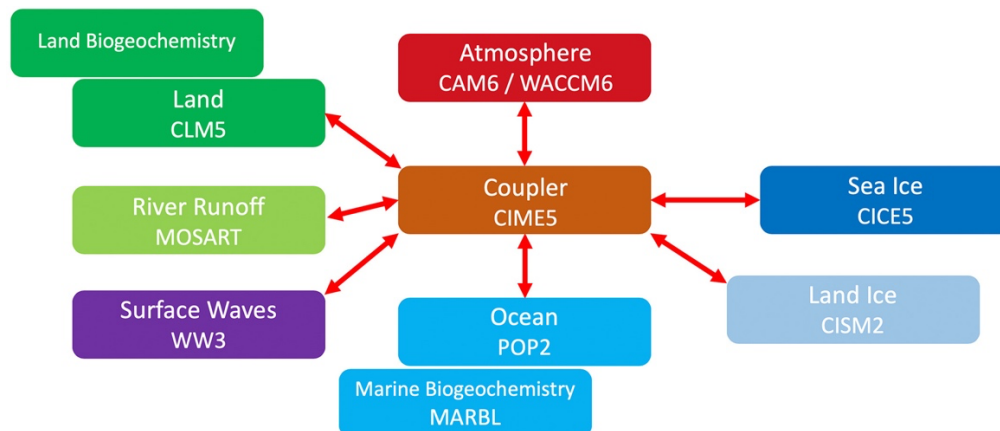


Figure 3: Schematic of the CESM2 component models (Danabasoglu et al., 2020).

Community Atmosphere Model (CAM)

The main focus of this project is on land-surface and plant-physiological responses to higher CO₂, which are represented in the Community Land Model (CLM), but the changes to the surface energy balance (i.e., radiative and turbulent fluxes, temperature, and humidity) are influenced via coupling with the atmosphere. The atmospheric component in CESM1 and CESM2 is the Community Atmosphere Model version 4 (CAM4) and 6.3 (CAM 6.3), respectively (Hurrell et al., 2013; Danabasoglu et al., 2020). Radiation in both versions of the model is parameterized using the Rapid Radiative Transfer Model for General circulation models (RRTMG). This parameterization is simplified for computational efficiency, yet has demonstrated accuracy for both longwave and shortwave radiation when compared to other models (Iacono et al., 2008). Importantly for this work, CAM can be configured with prescribed

changes in CO₂ concentrations both in line with and independently from the CLM. These models also export data on the same 0.05° resolution, allowing for the comparison of data exported from both models to be compared on the same scale.

Community Land Model (CLM)

The rates of evapotranspiration, and its components, canopy transpiration, canopy evaporation, and ground evaporation, are modelled in CESM1 by the Community Land Model version 4 (CLM 4) (Lindsay et al., 2014) and in CESM2 by version 5 (CLM5) (Danabasoglu et al., 2020). Both versions of CLM are used to integrate the terrestrial contributions and responses to weather, climate variability, and climate change. An update from CLM4 is that CLM5 includes a mechanism for plant hydraulics and hydraulic redistribution scheme, which models water transport through roots, stems, and leaves according to a simple hydraulic framework. It also includes an updated model of stomatal conductance, which includes both an optimal and empirical approach to modeling the biological process. In particular, a new parameterization of transpiration has been added to CLM5 to model the exchange of moisture between the land and atmospheric (Lawrence et al., 2019). CLM5 used the Medlyn model (Medlyn et al., 2011) to estimate stomatal conductance, the process that drives changes in evapotranspiration, based on vapor pressure deficit and CO₂ concentration. The Medlyn parameterization combines an empirical approach, based on experimental observations in response to environmental conditions, with an optimal approach, based on the theoretical argument that the stomata should act to minimize the amount of water used per unit carbon gained. CLM4 used the Ball-Berry Model (Ball et al., 1987), which is an empirical approach to represent transpiration from stomatal conductance that depends on the relative humidity and CO₂ concentration. This approach assumes that plants sense the relative humidity in the atmosphere rather than transpiration and/or

peristomatal water. Because both empirical and optimal modeling approaches have their own set of specific benefits, the updated Medlyn model seeks to build upon both. Relevant to this study, Kala et al. (2016) compares the effectiveness of the Medlyn model to the Ball-Berry model in modeling heatwaves. Experimenting under RCP8.5, their analysis revealed that the Medlyn model leads to an increase in the warmest yearly maximum temperature of 5°C in widespread regions, when compared to results from the previous model.

Coupled Model Intercomparison Project DECK and C4MIP Experiments

This study is based on output from the Coupled Model Intercomparison Project Phases 5 and 6 (CMIP6) (Taylor et al., 2012; Eyring et al., 2016), specifically the Diagnostic, Evaluation, and Characteristics of Klima (DECK) and Coupled Climate-Carbon Cycle Model Intercomparison Project (C4MIP) Experiments. Two simulations were used from the DECK experiment: an 1850 pre-industrial control simulation (*pi-control*, referred to from this point as pre-industrial) and a simulation forced by a 1% per year increase in CO₂ (*1pctCO2*, referred to from this point as FULL). *1pctCO2* is branched from the *pi-control* and the global mean CO₂ concentration increases at a rate of 1% per year until it reaches 4x the pre-industrial value over 140 years (Eyring et al., 2016)

This research also assesses specialized simulations from C4MIP, which are similar to the *1pctCO2* simulation described above. The C4MIP experiment was designed to analyze carbon cycle feedbacks and interactions in climate simulations (Jones et al., 2016) The C4MIP simulations aim to isolate the sensitivity of each of the components of the carbon cycle to climate and CO₂ changes separately. The additional C4MIP simulations include a simulation with only the carbon cycle components, not radiative effects, experiencing rising CO₂ (biogeochemically coupled, referred to from this point as the physiological simulation; PHYS) and a simulation

with only the radiation model components experiencing the rising CO₂ (radiatively coupled; RAD) (Jones et al., 2016). Altogether, the four simulations analyzed here included PRE-INDUSTRIAL, FULL, PHYS, and RAD, from both CESM1 and CESM2. A graphical representation of these simulation that demonstrates which component is being forced and which is being held constant at pre-industrial levels, is seen below. (Figure 4)

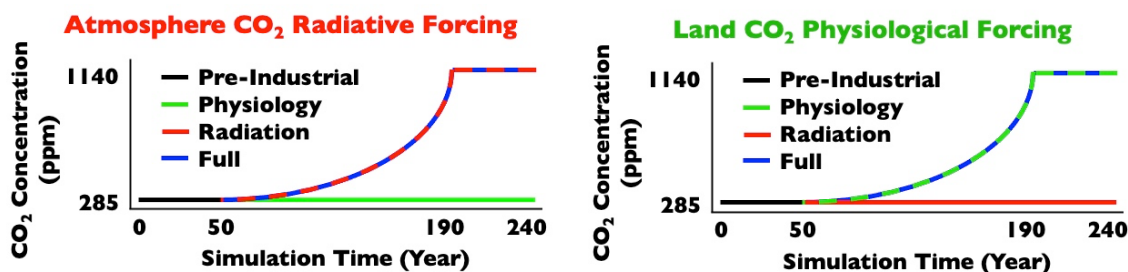


Figure 4: Graphical Representation of the C4MIP simulations

Unfortunately, output from the CESM CMIP5/6 simulations is only available for limited temporal resolutions, primarily monthly for most variables. To facilitate analysis of higher frequency temperature and heat index extremes, these simulations were extended at fixed 4x pre-industrial CO₂ concentrations starting from the end of year 140. CESM1.0.6 was extended for an additional 50-years and daily output was saved, while CESM2.2 was extended for an additional 20-years and daily and hourly output was saved. The additional CESM2 output provides an opportunity to determine if there is a significant difference between calculations of the heat index on hourly versus daily timescale due to nonlinearities in the diurnal cycle. Additionally, these extension simulations allow the climate system to more fully adjust to 4xCO₂ conditions.

Temperature and Heat Index Extremes

In this study, I primarily focus my analysis of the how the different CESM C4MIP simulations influence future projections of temperature, humidity, and the Heat Index (HI). HI is a measure of how hot it feels when relative humidity (RH) is factored in with the actual air temperature (NOAA, 2021). The computation for HI was modeled after Steadman’s apparent temperature, which includes dry bulb temperature and relative humidity to determine what this combination “feels like” to the typical human (Steadman, 1979). The main equation for HI is:

$$\text{HI} = -42.379 + 2.04901523 * T + 10.14333127 * \text{RH} - .22475541 * T * \text{RH} - .00683783 * T * T - .05481717 * \text{RH} * \text{RH} + .00122874 * T * T * \text{RH} + .00085282 * T * \text{RH} * \text{RH} - .00000199 * T * T * \text{RH} * \text{RH}$$

(Source: NOAA, 2014)

where T stands for temperature, and RH relative humidity. The units for heat index are the same as the input temperature, either °C, °F, or K depending on the analysis. To represent “extreme” temperature and heat index values as well as the mean, 99th percentiles are used. This threshold was chosen based on a number of studies of extreme heat that use 99th percentiles to signify “extreme” temperatures, such as Horton et al., 2016 and Lorenz et al., 2019. Additionally, the National Weather Service (NWS) has created a series of classifications that correspond HI values and the effects these values will have on the human body (Figure 3). Additionally, this analysis will include counts of the number of days in each of previously defined classifications for risks associated with heat index; and how they change due to FULL, PHYS, and RAD CO₂ forcing mechanisms.

CHAPTER 4

RESULTS

PART 1: Determining the necessity of hourly temperature and humidity data to calculate the heat index and its response to climate change

Previous studies (Bernhardt et al., 2018; Lee & Brenner, 2015) emphasize the importance of assessing the heat index on sub-daily timescales, since the diurnal cycles of temperature and humidity often have opposite patterns (i.e., relative humidity declines as temperature increases) and the heat index formulation is a nonlinear combination of these terms. However, sub-daily hourly output is rarely available from long-term earth system model simulations, such as CMIP5/6 experiments. It is therefore necessary to assess the degree to which calculating the heat index hourly differs from calculations with available daily timescale data. To illustrate whether hourly temporal scale temperature and humidity data is necessary for an accurate calculation of the heat index, I used 10-years of output from CESM2.2 pre-industrial and 4x pre-industrial CO₂ via the FULL 1pctCO₂ per year simulations. This allows for a comparison of both the pre-industrial baseline climate and climate change signals.

To determine the magnitude of the difference between daily and hourly heat index calculations, two different averaging techniques were used. The first technique took the 24hr average of temperature (T) and relative humidity (RH) data to calculate daily heat index (HI), which from this point on will be referred to as the “daily” calculation. The second technique calculated HI from T and RH at each hour, then averaged the 24-hour HI values to the day, referred to as the “hourly” calculation. Both of these result in daily HI values, however the first

represents the calculation that would come from standard daily model output. This comparison aims to determine whether there is a significant difference when calculating heat index given higher temporal T and RH data.

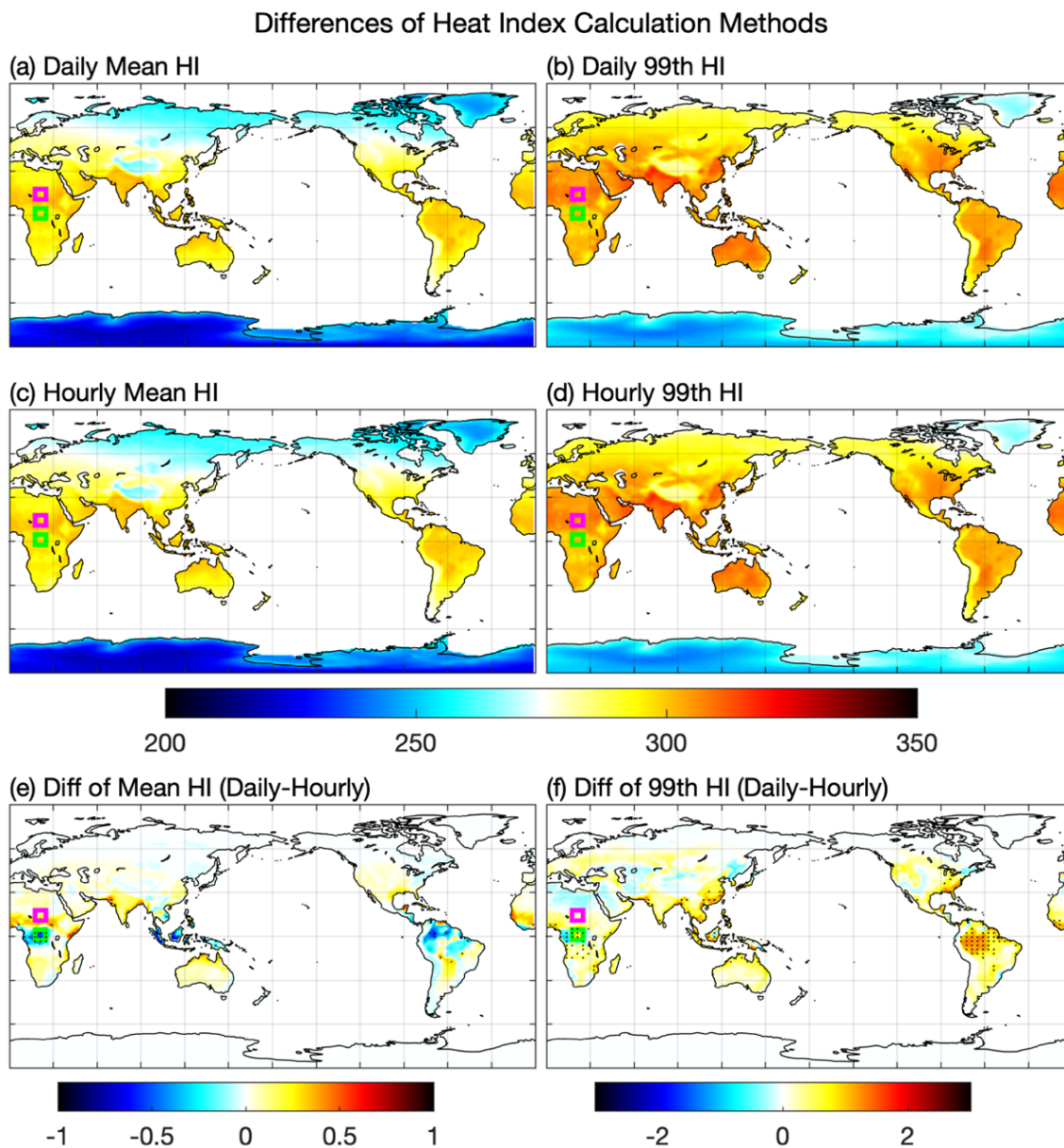


Figure 5: Pre-Industrial HI calculated using daily T and RH data (a) Mean from daily data (b) 99th percentile from daily data (c) Mean from hourly data (d) 99th percentile from hourly data HI Difference of Daily-Hourly calculations (e) Mean (f) 99th Percentiles. Stippling represents significance at the 95th percentile.

Overall, the geographic patterns of mean and extreme HI are very similar for both calculations (Figure 5, top and middle rows). The difference plots (bottom row) show that averaging either daily or hourly can lead to up to 2 degrees of difference of both the mean and 99th pre-industrial heat index in some regions. For the mean (left column), calculating the heat index daily can lead to values up to 1 degK cooler than if calculated hourly, with majority of this difference located in humid tropical forest regions. In the extra-tropics and beyond, general trends show that calculating daily will lead to warmer HI; though the magnitudes of this difference are not as great as with the difference in the tropics. Most regions where HI is higher when calculated daily are only warmer by approximately 0.2 degK, with the exception of the Sahel.

As for the 99th percentile heat index values, the majority of regions, including the tropics, show higher values when calculated daily. The region with the highest and most broad-scale difference is the northwest Amazon, where calculating daily leads to values 1 degK or greater than calculating hourly. Of note, this, and other tropical forest regions, had cooler values when calculated daily for mean HI. This flip between the mean and 99th percentiles implies the daily HI frequency distributions may be slightly cooler on average but broader (with higher extreme values) when calculated at daily timescales in these humid regions. In contrast, the dry Sahara has slightly warmer mean heat index values when calculated daily, but the 99th percentile daily values are lower than the hourly calculation. The same is true of most dry desert regions. I investigate these differences, and why there is a flip in some regions for mean and 99th percentiles, by looking more closely at a couple selected regions below (i.e., the pink box in the Sahel, a semi-arid region south of the Sahara Desert; and the green box in central Africa, a region generally dominated by tropical forests). However, I emphasize that these differences are

small compared to the main features of the baseline spatial patterns (left and middle columns), which are broadly similar with the two calculations.

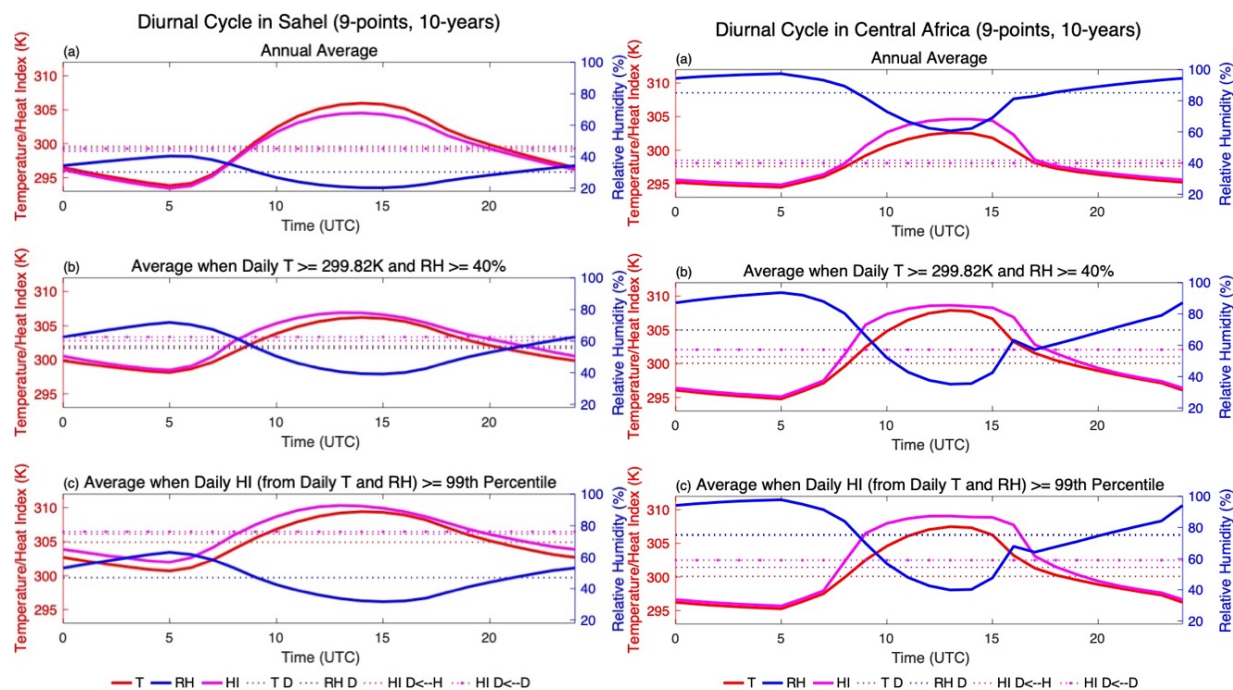


Figure 6: Diurnal Cycles the Sahel region. Parts a,b,c correspond to calculations of the heat index under different conditions. (D signifies daily, H signifies hourly)

Figure 7: Diurnal Cycles of Central Africa. Parts a,b,c correspond to calculations of the heat index under different conditions. (D signifies daily, H signifies hourly)

To investigate why there are differences between hourly vs. daily calculations of heat index, as well as why these differences flip between the mean and the 99th percentile, I have plotted the diurnal cycle of temperature, relative humidity, and heat index under different conditions. The top panels (a) of Figures 6 and 7 are the average diurnal cycles including all times, while the middle (b) and bottom (c) panels are only for days with high mean temperature and humidity (b) or HI values equal to or greater than the daily 99th percentile (c). The middle panels (b) constrain the calculation only for days when the standard HI regression equation is considered to be within valid bounds, i.e., for temperatures above 80°F (~299.83 degK) and relative humidity greater than 40%. For values not in that range, two adjustments are used. They

include one used when $RH < 13\%$ and temperature is between 80 and 112°F; and another for when $RH > 85\%$, and temperatures are between 80 and 87°F. For all other values, a simpler formula is used. The bottom panels (c) indicate that days greater than the 99th percentile tend to overlap with days when the standard HI regression equation is valid.

The result shows that the heat index, when calculated from all days, can lead to values that are less than the temperature in the Sahel (Figure 6a). This is due to the very low values of relative humidity, with averages well below the standard 40% threshold. This result is valid and discussed on the National Weather Service Amarillo page (NWS, 2019), but does not necessarily relate to the process of interest here associated with the influences of plants on climate and human impacts. This is not an issue for the Central African region, where the majority of days have RH values exceeding 40% (Figure 7a). It is also not an issue for the Sahel region when considering days with values above the specified thresholds and high values of HI (Figure 6b,c), which have the primary impact on changes in extreme events.

Focusing on these higher HI value days, the comparison between these two regions is more straightforward. In both regions, higher HI days selects for higher temperature days (panels b and c versus a). For the Sahel (Figure 6b,c), this also selects for higher relative humidity days, but for Central Africa (Figure 7b,c), which is overall much more humid, this reduces the values of mean relative humidity. Since RH is temperature dependent, lower temperature days lead to higher relative humidity when all days are considered (Figure 7a).

More importantly, the diurnal cycle plots demonstrate that the high values of temperature and RH do not occur during the same hours of the day, which is lost when calculating HI from daily temporal scale data. This may also be due in part to the non-linearity of the HI calculation. Because of this, there are small differences in HI values calculated from daily rather than hourly

data. This is most evident in Central Africa (Figure 7b), where the difference in HI is about 1 degK higher for the daily calculation (dash-dotted purple line versus dotted purple line). The larger differences in Central Africa are likely due to the larger diurnal cycles of temperature (~13 degK range) and relative humidity (55% range) compared to the Sahel (~8 degK and ~30% ranges). Due to nonlinearities in the heat index equation, the high humidity regime in Central Africa can also exert a great influence on HI. This primarily occurs in the morning and late afternoon, when RH and T are moderately high, but decreases in mid-day with RH drops (Figure 7b). This pattern is also seen in the Sahel but to a lesser extent (Figure 6b). That being said, while the differences in the HI calculation have a small impact on the absolute values, the signals are generally consistent. Even for the Sahel, including all days (Figure 6a), where the HI diurnal cycle is lower than T, the daily mean HI is lower than daily mean T consistently for both calculations (both horizontal purple lines are lower than the horizontal red line, though the differences are difficult to distinguish visually).

Similar results can be seen in the daily distributions of heat index calculated with both methods (blue versus teal bars in panels (f) of Figures 8 and 9). In the Sahel (Figure 8f), there are very similar distributions between the temporal averaging methods, with differences in the mean and 99th percentile of +0.3 and +0.2 degK when calculated from daily data, respectively. For Central Africa (Figure 9f), the differences are slightly larger and opposite for the mean (-0.5 degK) and 99th percentile (+0.6 degK) when calculated from daily data relative to hourly. However, like the spatial distributions, main features of these results (and difference between regions) are evident with both methods.

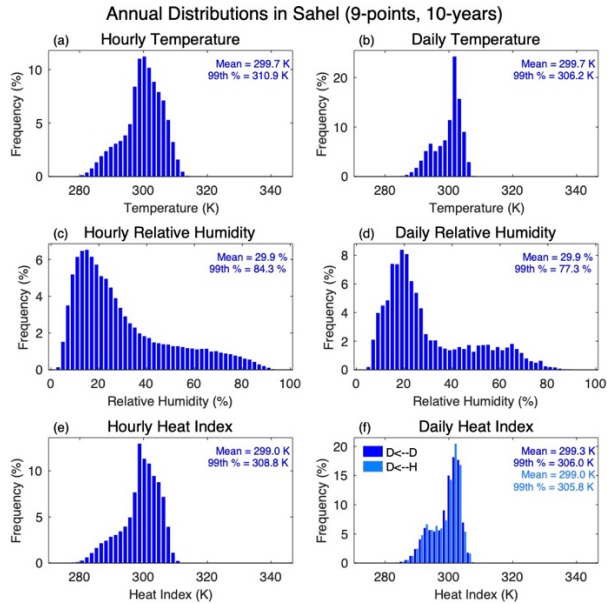


Figure 8: Distributions of hourly and daily temperature, relative humidity, and heat index for the Sahel region.

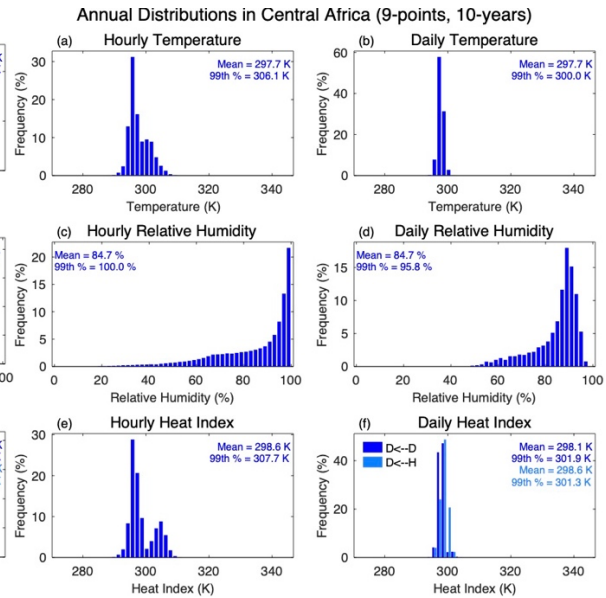


Figure 9: Distributions of hourly and daily temperature, relative humidity, and heat index for the Central African region.

To investigate further what is behind these distributions, I also assessed distributions of temperature and relative humidity, on hourly and daily timescales. For both regions, the Sahel and Central Africa, distributions between hourly and daily temperature and relative humidity data are very similar, with daily values narrowed relative to hourly (Figure 8 and 9). These plots also demonstrate the differences of the climates of the two regions. The Sahel sees higher frequencies of days with daily averages below 40% relative humidity; whereas Central Africa sees majority of days with $RH > 60\%$.

For HI, there is evidence of a bimodal pattern, which is not present within the temperature or RH data, but results from the calculation of heat index. This is most evident in the hourly HI distribution for Central Africa. As previously stated, the heat index calculation contains a number of adjustments based on values of temperature and relative humidity, one of which occurs at 80°F , or approximately at 300 degK. This explains the dip in the Central African

distribution (Figure 9e). This dip is less evident in the daily HI distribution (Figure 9f) with the broad bin spacing used, but appears when the HI distribution is calculated from daily data using finer bin resolution (Figure 10). As temperatures approach this threshold, values are shifted left or right, leading to the lower frequencies around this point. The reason this is more prevalent within the hourly distributions (or daily from daily heat index calculation) is because the daily mean values calculated from hourly data smooth out this effect.

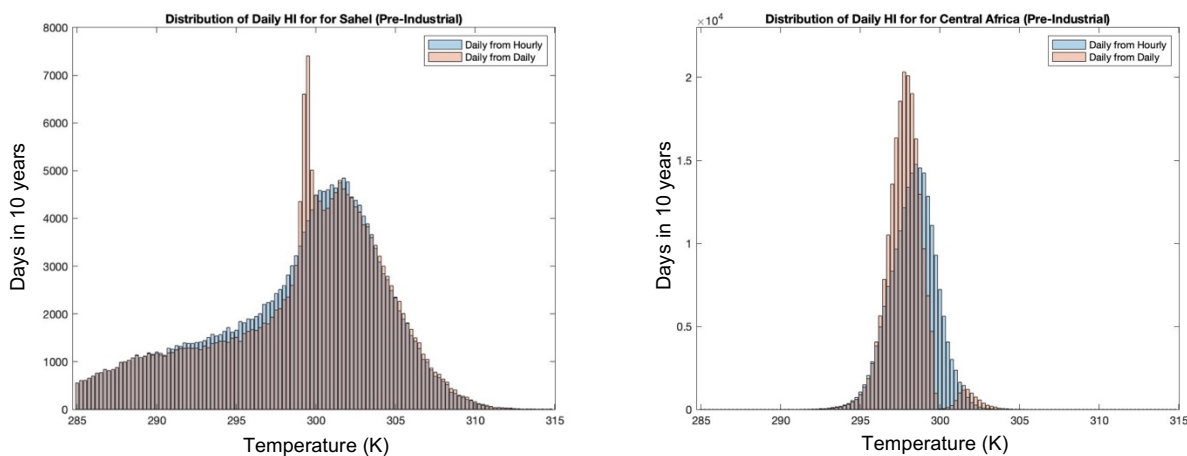


Figure 10: Distributions of hourly and daily heat index, for the (left) Sahel and (right) Central African regions. Similar to Figures 7f and 8f, but with finer bin spacing and for one gridbox.

The previous analysis has analyzed the affect that hourly vs. daily analysis within a single climate, the pre-industrial. The following figures analyze the impact on the change in the heat index. For this investigation, I use data from the CESM2 4xCO₂ extension run described above in methods. The analysis into the difference of the overall change (Figure 11) produces similar conclusions to those in the pre-industrial climate, i.e., the bulk of the signal is similarly captured by both methods, with only small differences. In this case, daily data yields higher values for both the mean and 99th percentiles. The highest of these values is only approximately 1degK warmer than that of the hourly values for the mean, about 5% of the overall change. Regions in the tropics that had lower mean values for the pre-industrial climate with the daily calculation,

have higher mean values for the change. There are a couple regions where there is a flip in sign from mean to 99th percentile (e.g., the America Rockies), but general the sign of the difference in the change is positive everywhere. For the 99th percentile, the differences are a larger, up to +3 degK in some isolated regions, but broadly, the differences are less than a degree. These similarities are also seen for the changes in the heat index distributions as calculated by both methods (Figures 12f and 13f), even for the Central Africa region which appears a large mean difference in the spatial plots (Figure 10c).

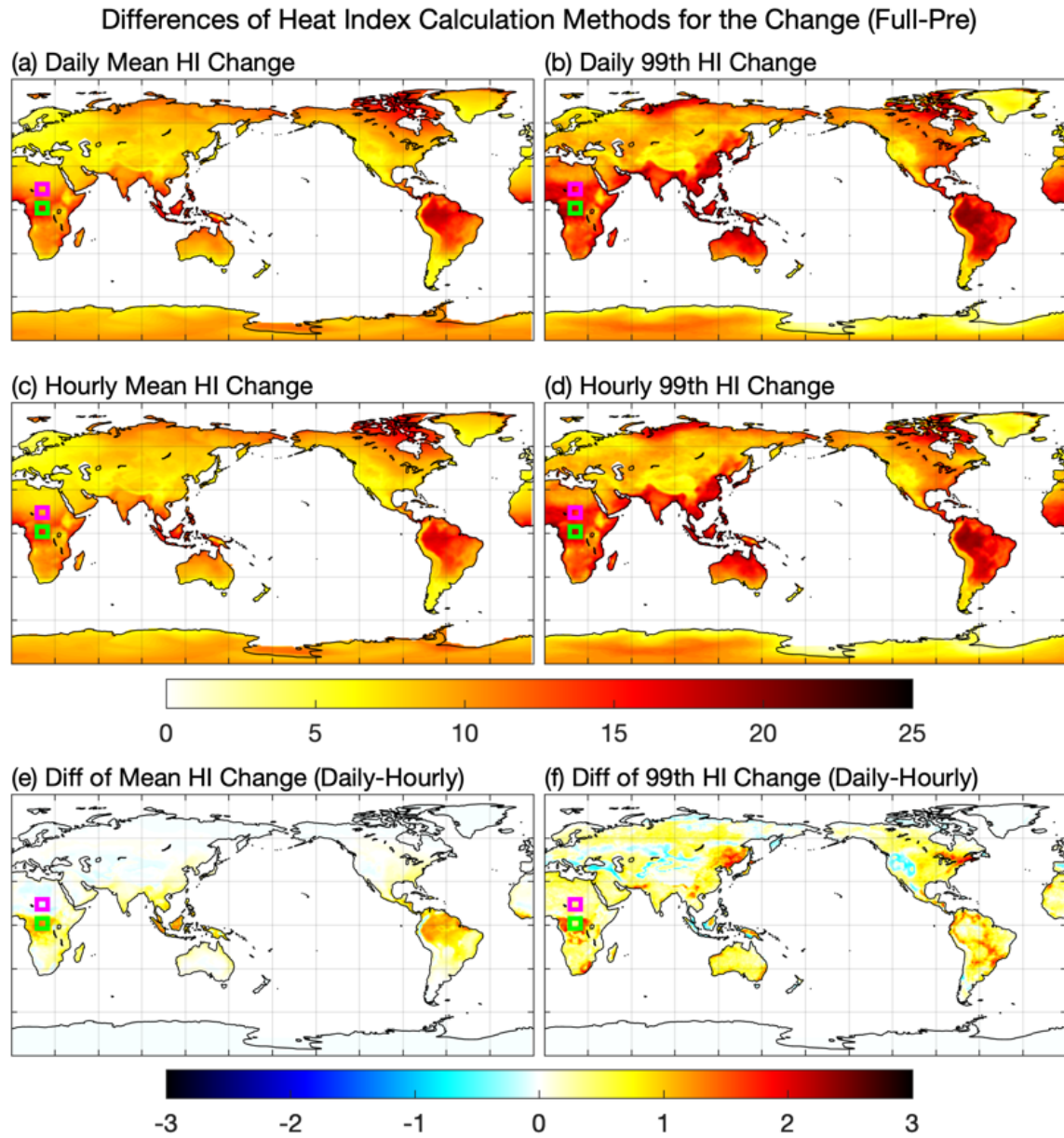


Figure 11: The change of HI from the pre-industrial climate to a fully coupled rad & phys simulation, calculated using daily T and RH data (a) Mean (d) 99th Percentiles. HI calculated hourly, then averaged to the day (b) Mean (d) 99th Percentiles. Difference of Daily-Hourly calculations of the change (c) Mean (f) 99th Percentiles. Stippling represents significance at the 95th percentile.

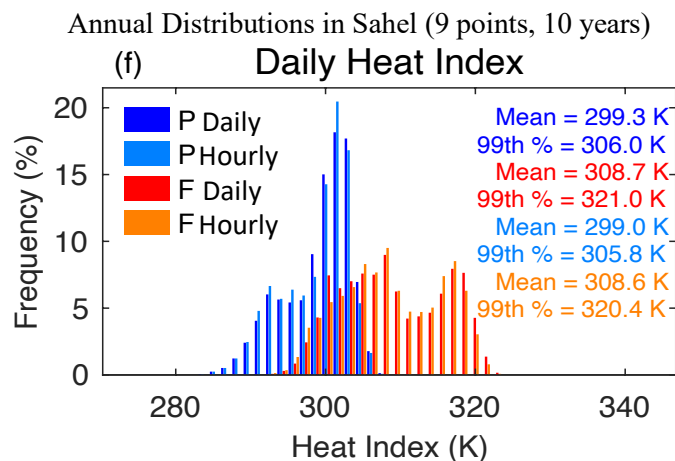


Figure 12: Distributions of daily HI for the Sahel region from pre-industrial (P) and full (F) simulations.

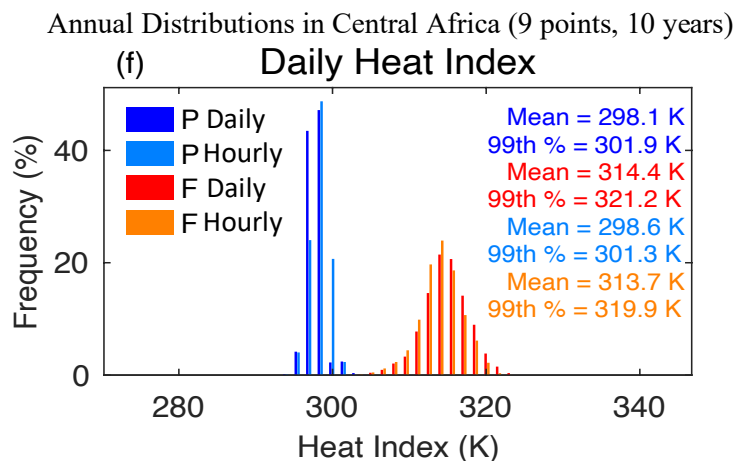


Figure 13: Distributions of daily HI for the Central African region from pre-industrial (P) and full (F) simulations.

Another to indicator of extreme heat events is the series of heat index classifications set up by the National Weather Service (NOAA, 2019). As introduced in the literature review, the NWS has set up a series of classifications (caution, extreme caution, danger, and extreme danger, Figure 2) for HI and the associated heat illness at given thresholds. Assessing changes to HI at these thresholds has the benefit of being defined equally for all regions; whereas the mean and 99th percentiles depend on the stats of that given area. In Figure 14, I assess the difference of hourly and daily calculation methods of HI in the pre-industrial climate. In the pre-industrial climate, there is an average of around 100-150 days per year being classified as “caution”. Results show that hourly data is leading to many more days being classified in the “caution” category (299.817 to 305.72 degK), with some regions seeing 75+ days/per year being classified with hourly data. The likely reason for this would be hourly data leading to higher temperatures, enabling more days to be to fall under NWS classification rather than be unclassified. The warmer the categories get, the less disparity there is between hourly and daily. This is not due to

agreement between calculation methods; but rather a lack of days defined at these thresholds in the pre-industrial runs.

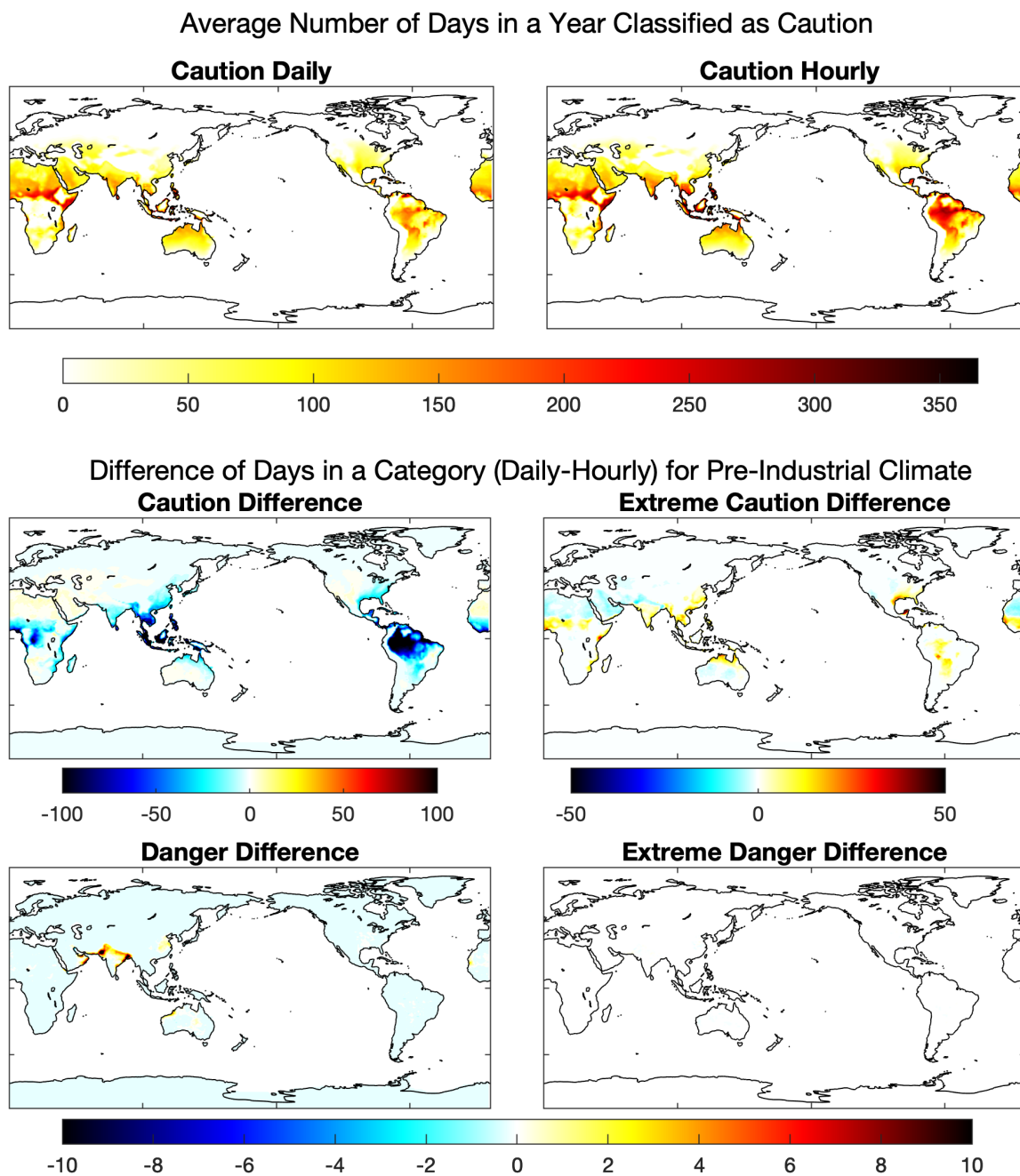


Figure 14: Averages and Differences of HI in NWS defined categories of daily vs. hourly data

The results of the difference of hourly and daily within the full change from pre-industrial for the NWS categories (Figure 15) show notable differences from just the pre-industrial. For both hourly and daily data, there are strong decreases in the number of caution days. As global temperatures increase, they would become reclassified in higher categories. This is confirmed by the counts of “danger” days, which are seeing an overall increase from pre-industrial. Within the caution difference, majority of the globe is seeing higher numbers of days due to hourly, but the warmer, wetter regions of the tropics see higher values when calculated daily. Danger differences are dissimilar, with more regions seeing higher counts when calculated daily, though higher hourly regions are still present. Extreme danger sees little to no difference between hourly and daily.

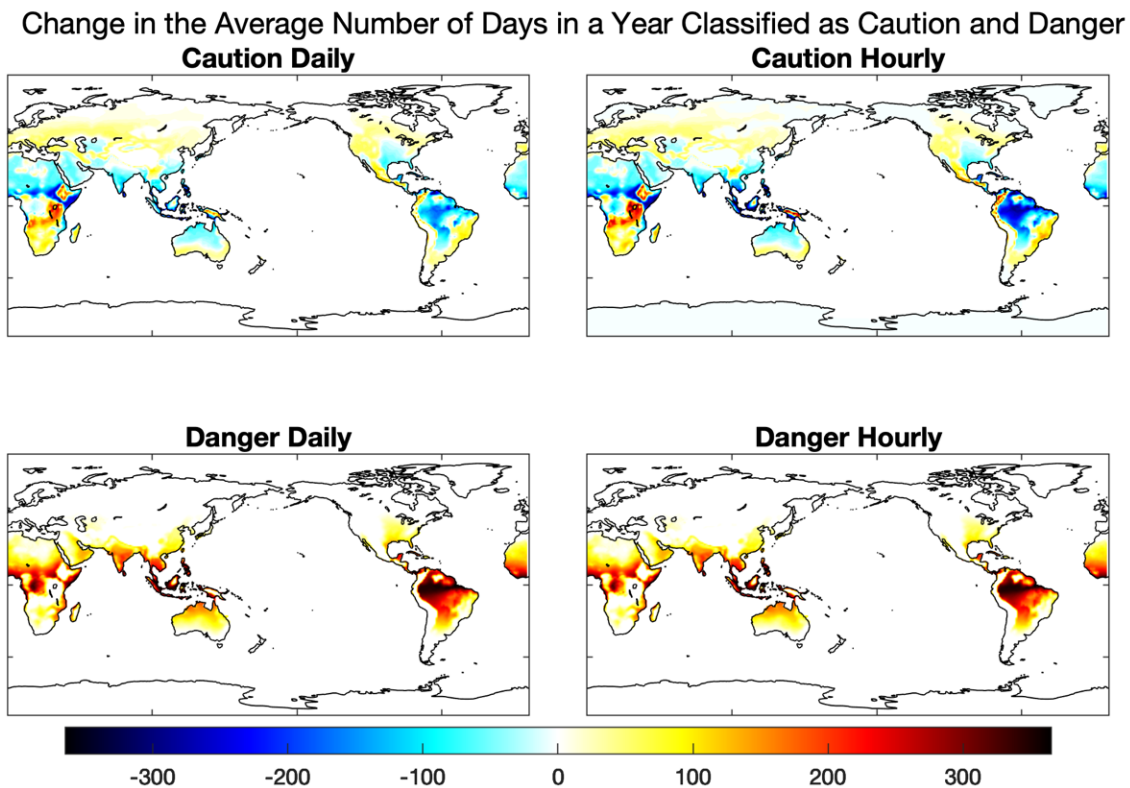


Figure 15: Average counts of the change in HI from the pre-industrial for hourly and daily, caution and danger categories.

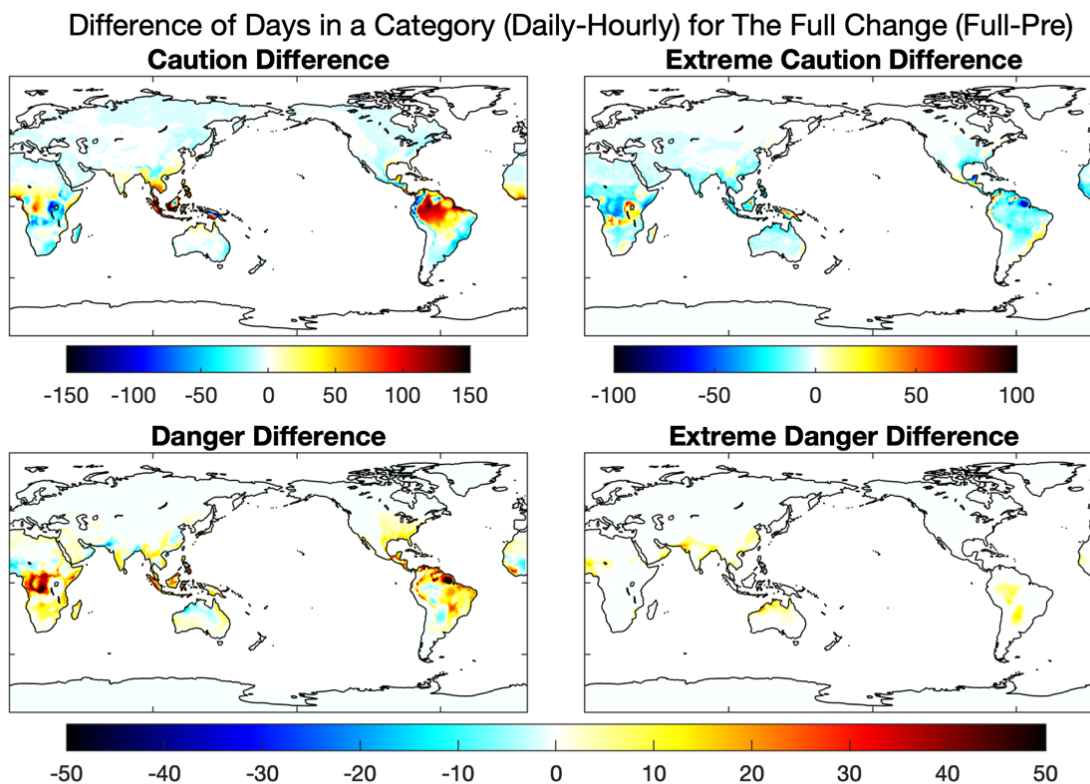


Figure 16: Differences of the change in HI from the pre-industrial to the full, of the NWS defined categories of daily vs. hourly data

In summary, there are some interesting differences when calculating the heat index from hourly vs. daily data, assessed here for the mean and 99th percentiles (as the heat index extreme metric). The NWS category counts show more notable differences, and I conclude future research using this metric should consider sub-daily scale T and RH data if available. However, in the analysis above, I have discussed the nuances of these difference, but overall conclude that the daily captures the majority of the signal and can be used to broadly in compare different model versions.

PART 2: Changes in the Heat Index and its Radiative and Plant Physiological Components under Increased CO₂ in the Community Earth System Model versions 1 and 2

Although nonlinearities in the diurnal cycles of temperature and relative humidity lead to small differences in the heat index when calculated at the hourly rather than daily timescale, the results of Part 1 highlight that the main features of the pre-industrial and climate change (Full minus pre-industrial) signals (spatial pattern and frequency distribution) are captured in daily analysis. This allows for a comparison across model versions for which only daily timescale output is available (i.e., typical temporal resolution of CMIP5/6 experiment data). For this study, I focus on a detailed comparison between CESM1 and CESM2, which represent several relevant differences in the representation of stomatal conductance and plant growth (described in Chapter 3: Methods above). In particular, updates in CESM2 lead to significant differences in LAI sensitivities to increasing CO₂, which modulate plant influences on the heat index. Part 2 (this section) quantifies the changes in the heat index as well as temperature and humidity, while Part 3 investigates the underlying plant physiological processes that drive those changes.

The following analysis is based on the 4x pre-industrial CO₂ extension periods of the C4MIP experiment design for both CESM1 and CESM2. As described earlier, CESM1 was run for a 50-year period after the climate reaches 4xCO₂ at a 1% per year increase. The extension holds CO₂ constant at the 4xCO₂ level, in order for the climate to more fully adjust to the elevated concentration and save additional output. The last ten years of that extension run is used for this analysis. CESM2 was run for a similar extension period, but only 20 years long; and this analysis used the last 10 years of that extension run. While the CESM1 extension simulation was longer, our offline analysis found that the climates had mostly adjusted to 4xCO₂ in both each model versions (in fact the warming in CESM2 Full/Rad-Only simulations is even greater than

CESM1, despite the shorter period, as shown below), and are similar enough to allow for comparison.

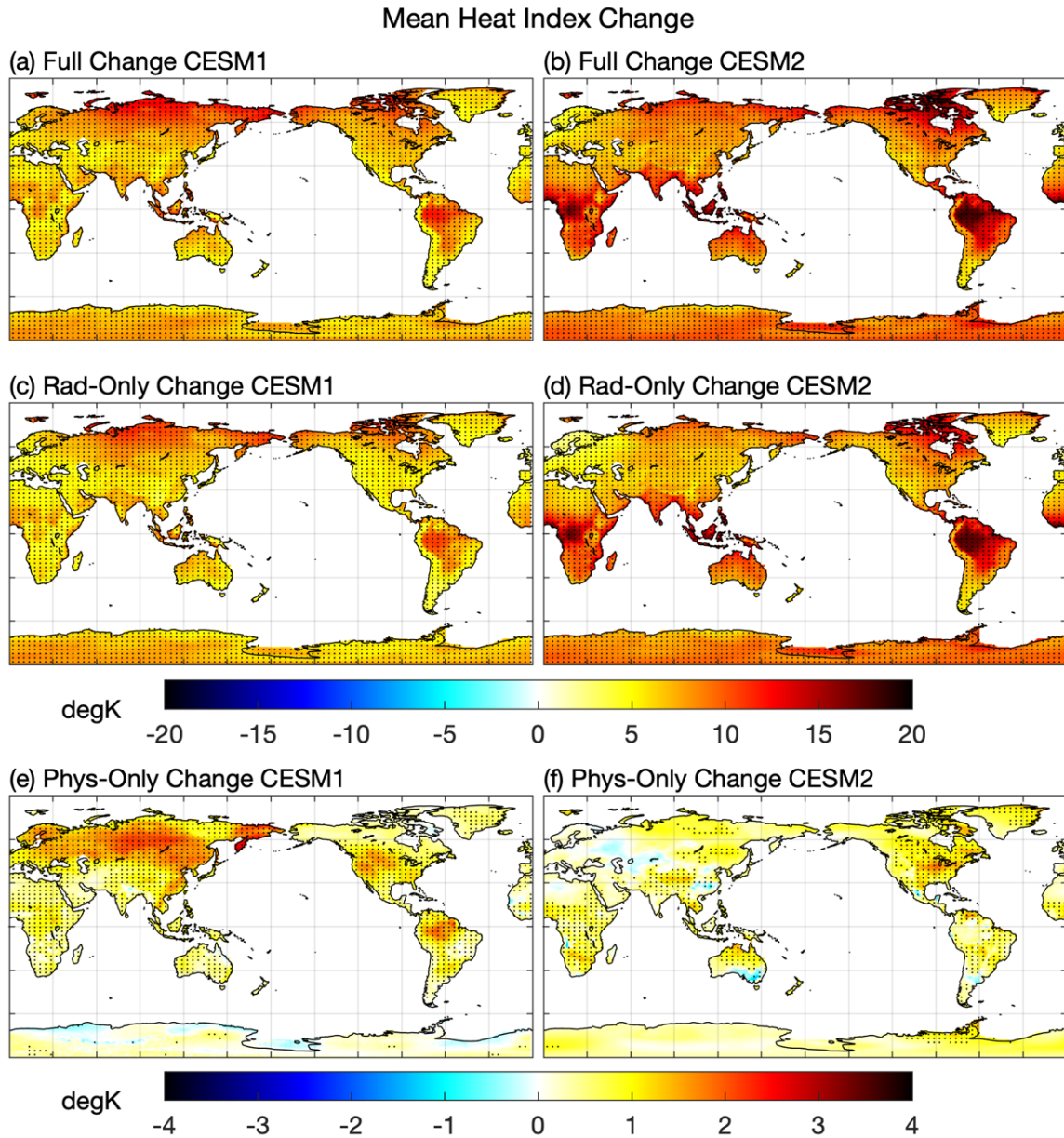


Figure 17: Changes of Mean Heat Index from the Pre-Industrial to the (a,b) Full (c,d) Radiation Only (e,f) Physiology Only Simulations. Stippling represents significance at the 95th percentile confidence interval. The top color bar corresponds to plots (a-d) and the lower to plots (e & f). Stippling represents significance at the 95th percentile.

Both CESM1 and CESM2 project significant warming of the heat index for both the full and radiation-only simulations (Figure 16). In CESM1, the highest values of the mean warming are around 10-15 degK, while in CESM2 they are in the range of 15-20 degK. This is consistent with a higher climate sensitivity in CESM2, at least 1.5 degK higher than CESM1 (Bacmeister et al., 2020). Majority of the warming in the full simulation of CESM2 is located in the tropics; whereas in CESM1 there are high levels of warming in the tropics and the high latitudes. Most of this warming in the Full simulations of both versions is attributed to the enhanced greenhouse effect, as seen by the Rad-Only change; and the higher radiative response in CESM2 is associated with stronger shortwave radiation feedbacks (Bacmeister et al., 2020). However, in CESM1 plant-physiological effects account for upwards of 2-3 degK of warming, notably over western North America, northern Eurasia and the Amazon. This accounts for ~20% of the increase in the Full simulation. Additionally, there is at least 1 degK of warming over all land. While these values of warming may seem small, they represent at least 10% of the overall Full change for all land areas, except for Antarctica. In CESM2, there is less warming due to physiology-only, with only a small area in the American Midwest increasing by over 1 degK. Most areas are warming slightly, but some areas, such as southeastern Australia and central Eurasia, are getting cooler under a physiology-only simulation in CESM2 (though these cooling regions are not statistically significant). The potential reasons behind this cooling will be further elaborated in Part 3.

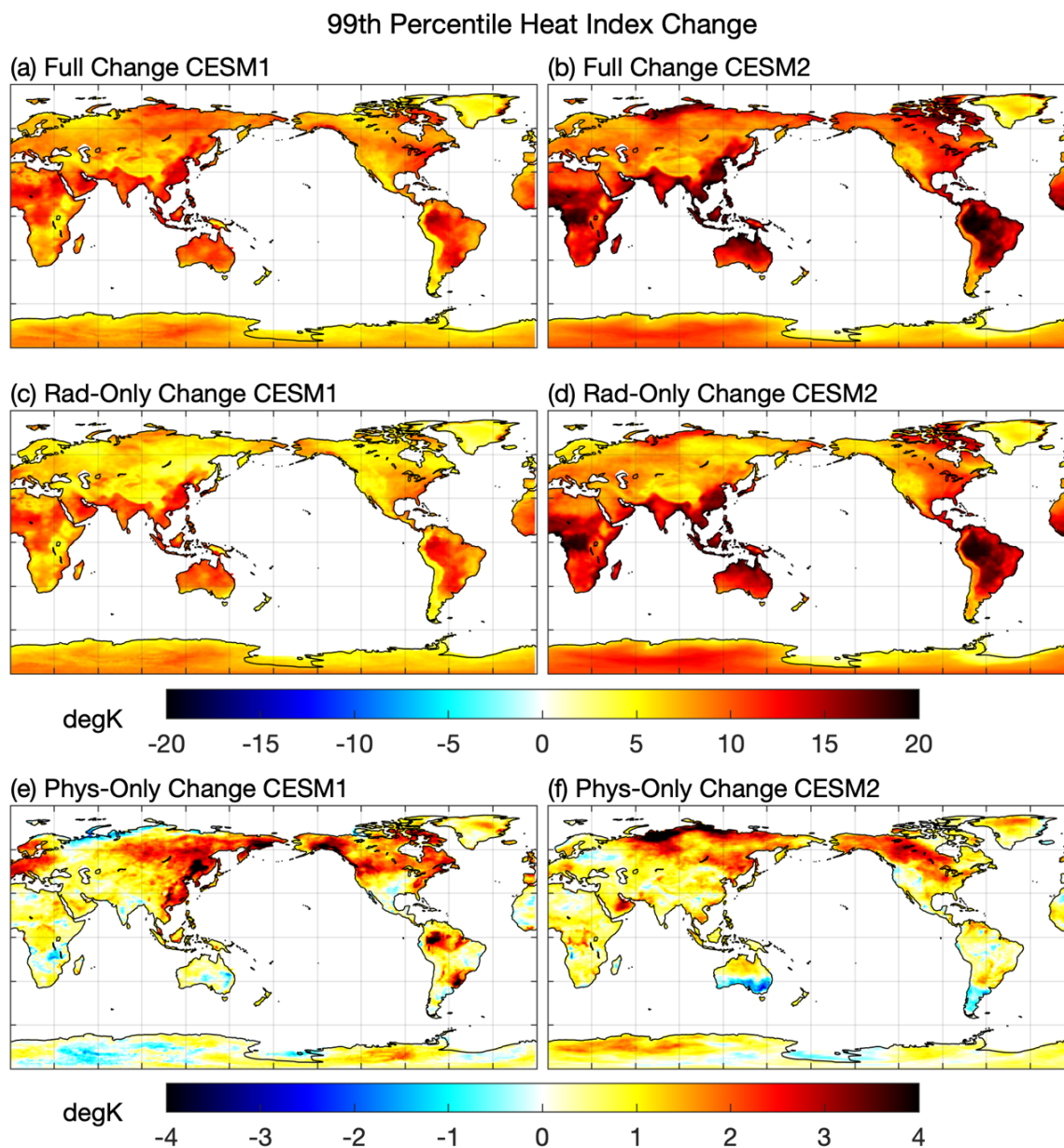


Figure 18: Changes of the 99th Percentile Heat Index from the Pre-Industrial to the (a,b) Full (c,d) Radiation Only (e,f) Physiology Only Simulations. The top color bar corresponds to plots (a-d) and the bottom to (e & f).

While it can be insightful to assess the annual mean changes, the heat index was designed and validated particularly for extreme heat events. Extremes are assessed here as changes in the 99th percentile heat index relative to the pre-industrial (Figure 17). The full and radiation simulations have consistent and globally homogeneous warming over all land areas, similar in

pattern to the mean changes. CESM2 shows greater warming, with some regions increasing 5 degK more than the change in CESM1. In contrast, warming by physiological forcing patterns are less spatially consistent, with some areas of cooling or warming. This is true of both model versions, though in general they both highlight the northern mid-high latitudes of North America and Eurasia for enhanced extremes. However, notable differences are the areas of warming in northwestern and southeastern South America in CESM1 that do not appear in CESM2; and along the arctic coast of northeastern Russia, which has a small cooling signal in the CESM1 Phys-Only simulation, but substantial warming in CESM2. Overall, the magnitude of physiology-only changes is similar for northern high-latitudes, despite small differences in the spatial pattern. However, since the radiative response is larger in CESM2, the relative contribution of physiology to the Full change is smaller.

It is also worth noting that the 99th percentile changes represent a relative change compared to pre-industrial, and may not necessarily result in absolute values that reach caution or dangerous levels to human health as defined in the HI classification chart (Figure 2).

The previous analysis investigated the mean and 99th percentiles, which vary in magnitude from region to region. To investigate changes in heat index at absolute metrics, I analyzed the changes in the counts of days/year falling within the NWS categories (Figure 18 and Figure 19). These results show similar findings to the mean and 99th percentiles of HI. In terms of overall warming in the full and rad-only simulations, CESM2 is showing more warming, with larger counts of days being classified in the combined danger/extreme danger category. Some regions in these simulations, notably the tropical equatorial regions, are seeing 200+ days in a year being classified in this category. This could have grave impacts for human health, as in these regions, more than half the year would be days where prolonged outside

exposure could lead to heat cramps, heat exhaustion, or heat stroke. CESM1 shows higher rates of days being classified in the combo caution/extreme caution category, which could still lead to heat exhaustion and possible heat stroke with long periods of outdoor exposure.

In terms of the Phys-only simulations, results are again consistent with the finding of the changes to mean heat index (Figure 16). Under CESM1, phys-only changes to heat index are higher than that of CESM2. In CESM1, maximum count values are in the upwards range of 100 days/year, mostly in north-central South America. In CESM2, there is a small region on the north coast of South America seeing a similar magnitude of change; but majority of the change seen globally is under 50 days/year. For both model simulations, there are very few regions seeing a change to days classified as danger/extreme danger, since the magnitude of warming in phys-only simulations is not high enough to yield HI values in these thresholds.

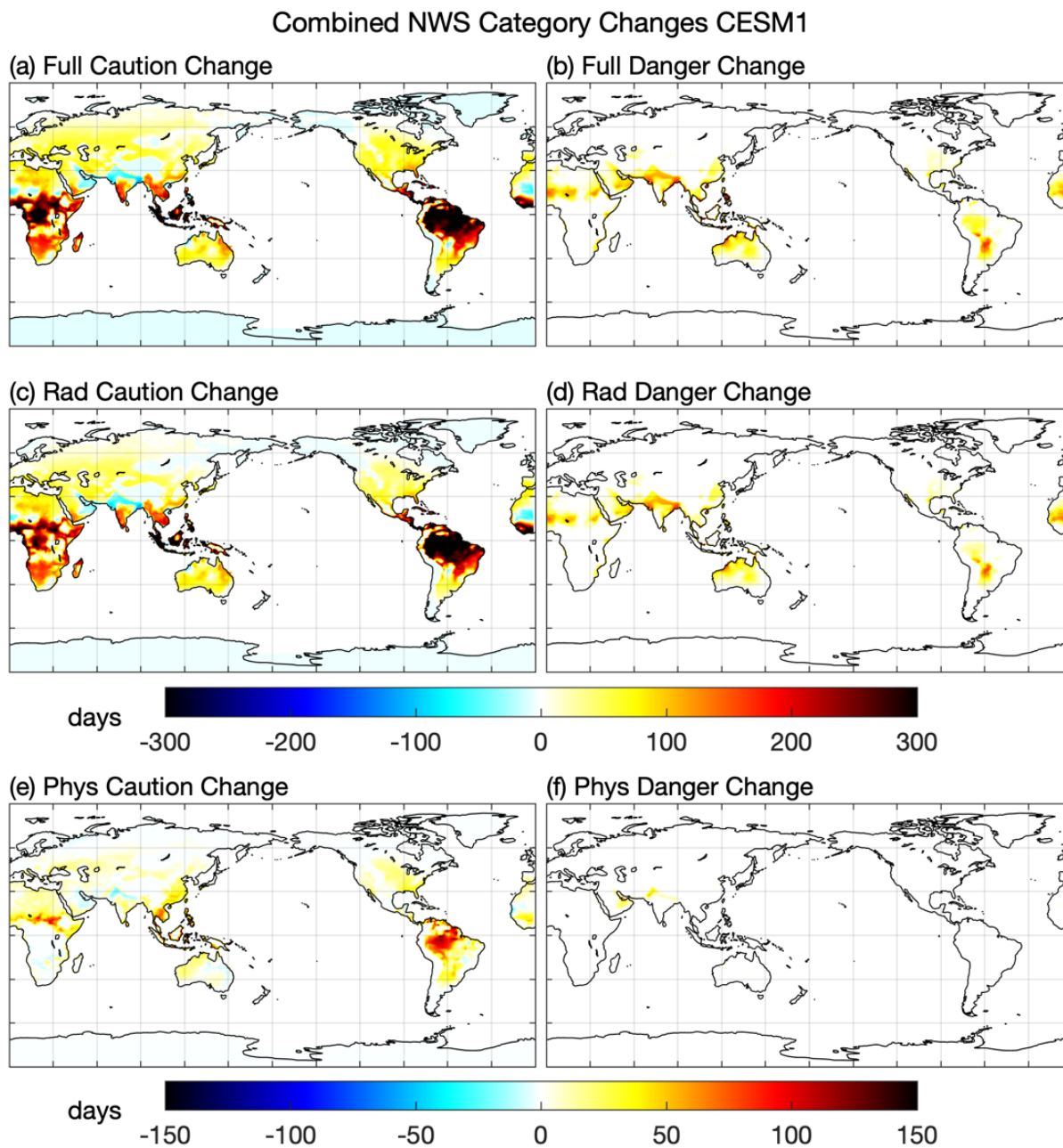


Figure 19: Changes in the counts of days in the defined NWS thresholds for the Full (a&b) Rad-Only (c&d) and Phys-Only (e&f) Simulations in CESM1 Note: Caution/Extreme Caution and Danger/Extreme danger counts have been combined in single categories. Unit: days/year.

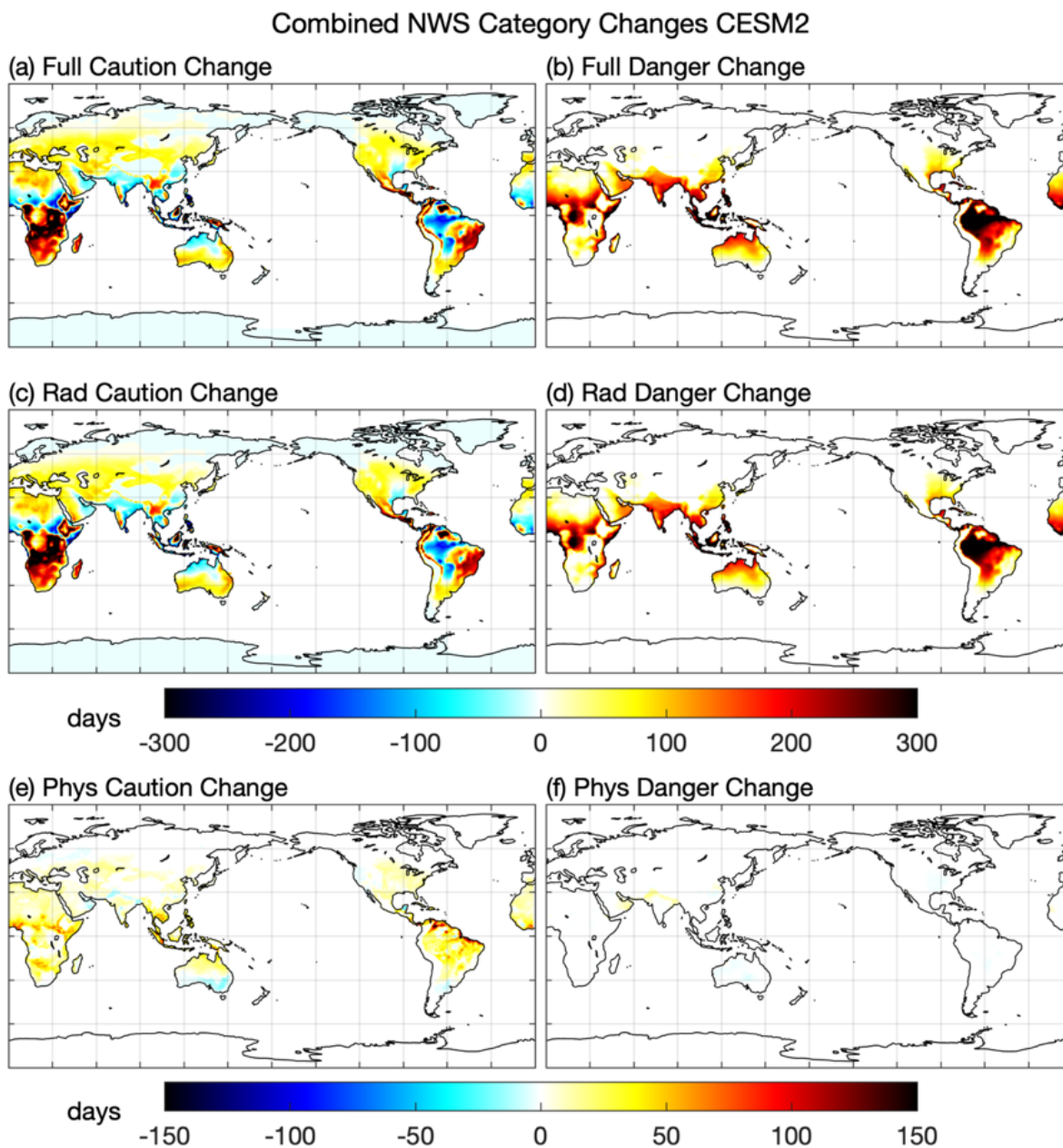


Figure 20: Changes in the counts of days in the defined NWS thresholds for the Full (a&b) Rad-Only (c&d) and Phys-Only (e&f) Simulations in CESM2 Note: Caution/Extreme Caution and Danger/Extreme danger counts have been combined in single categories. Unit: days/year.

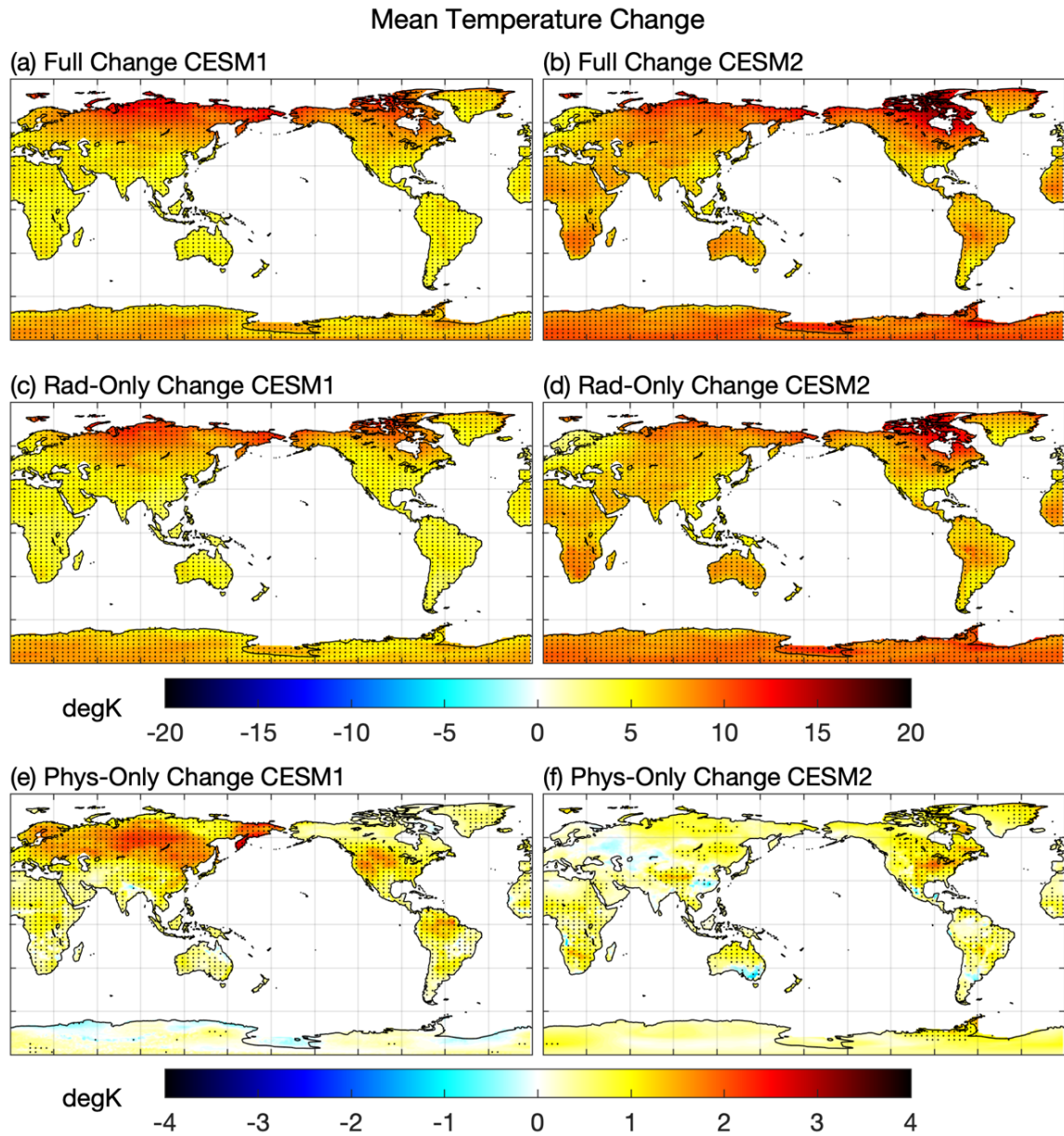


Figure 21: Changes of Mean Temperature from the Pre-Industrial to the (a,b) Full (c,d) Radiation Only (e,f) Physiology Only Simulations. Stippling represents significance at the 95th percentile confidence interval. The top color bar corresponds to plots (a-d) and the bottom to (e & f). Stippling represents significance at the 95th percentile.

To further investigate what is driving these changes in heat index, we first look at the temperature, the variable that has the main influence on heat index. Projections of temperature are thus expected to be similar to HI. The main differences when comparing mean changes in

these variables (Figure 16 versus Figure 20) is that temperature highlights polar amplification in the Full and Rad-only simulations, while heat index is also strongly influenced by high humidity and so, also highlights the tropics. In both CESM1 and CESM2, in the full and rad-only simulations, heat index warms by 5-10K more than the temperature in the tropics. In the phys-only simulations, the changes in spatial patterns between temperature and heat index in CESM1 and CESM2 are more similar to one another, with the same regions experiencing warming or cooling. A notable exception is the Amazon warming seen in the HI change is not as strong in the temperature change in CESM1. Additionally, like the HI, mean temperature changes show broader scale of warming that is larger in CESM1 than CESM2 in response to plant-physiology changes.

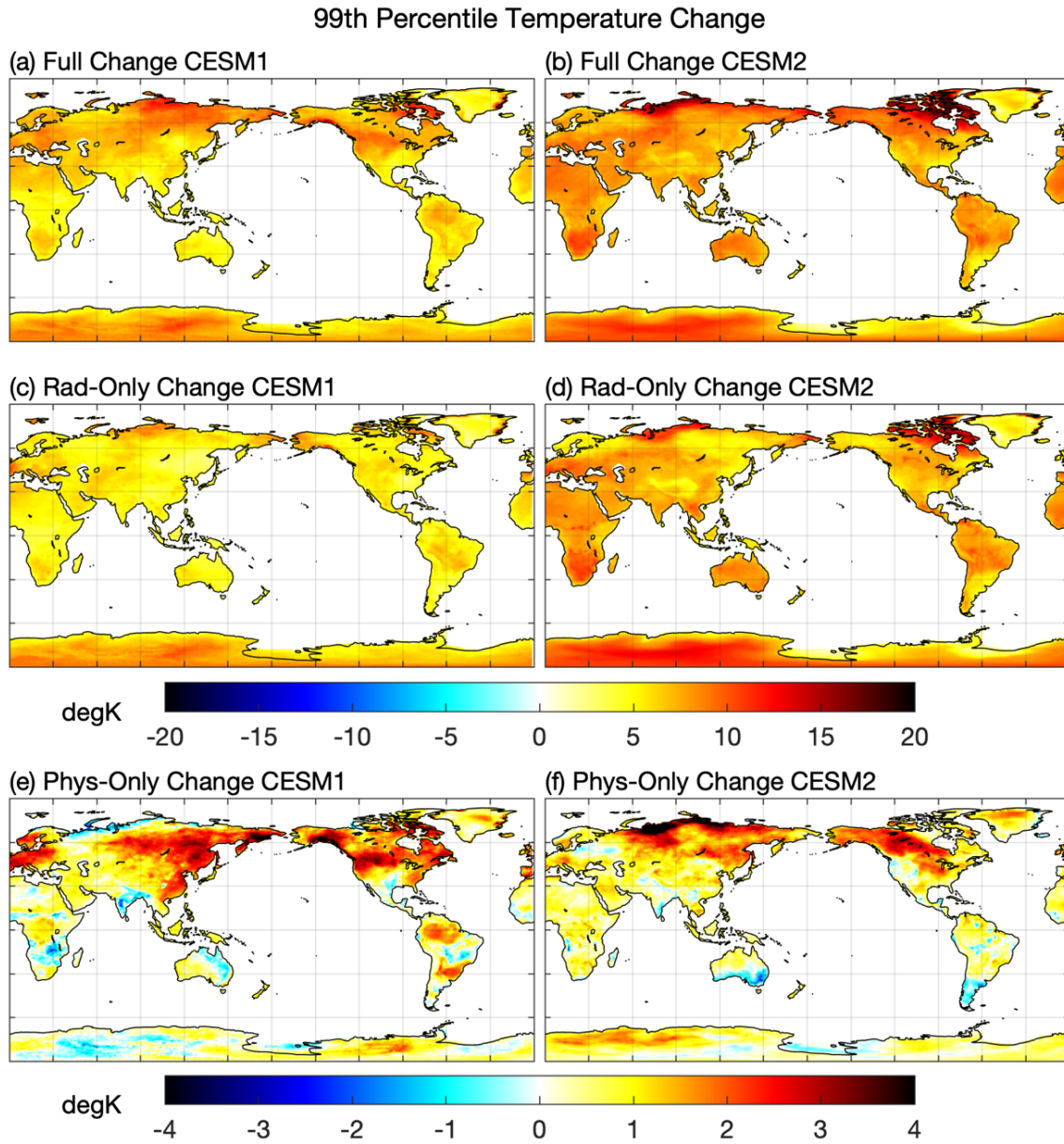


Figure 22: Changes of the 99th Percentile Temperature from the Pre-Industrial to the (a,b) Full (c,d) Radiation Only (e,f) Physiology Only Simulations. The top color bar corresponds to plots (a-d) and the bottom to (e & f).

Similar findings are also true for the 99th percentile of temperature changes (Figure 21). There is a general warming pattern of upwards of 10K for both the full and the rad-only change from pre-industrial, which is strongest in high-latitude regions. For the phys-only simulations, there are areas that experience an increase in 99th percentile temperatures and areas that

experience a decrease. Unlike the mean change, there are also broad areas where these values are mostly unchanged from the pre-industrial. This implies that physiology contributes to shifting the distribution of daily temperatures to higher values everywhere (at least in CESM1), but possibly narrowing the distribution (i.e., extremes do not increase as much) in some regions. In those regions, most of the warming of extreme temperatures results from the enhanced greenhouse effect, with smaller or offsetting effects (i.e., stomatal conductance versus LAI) from plant physiological forcing.

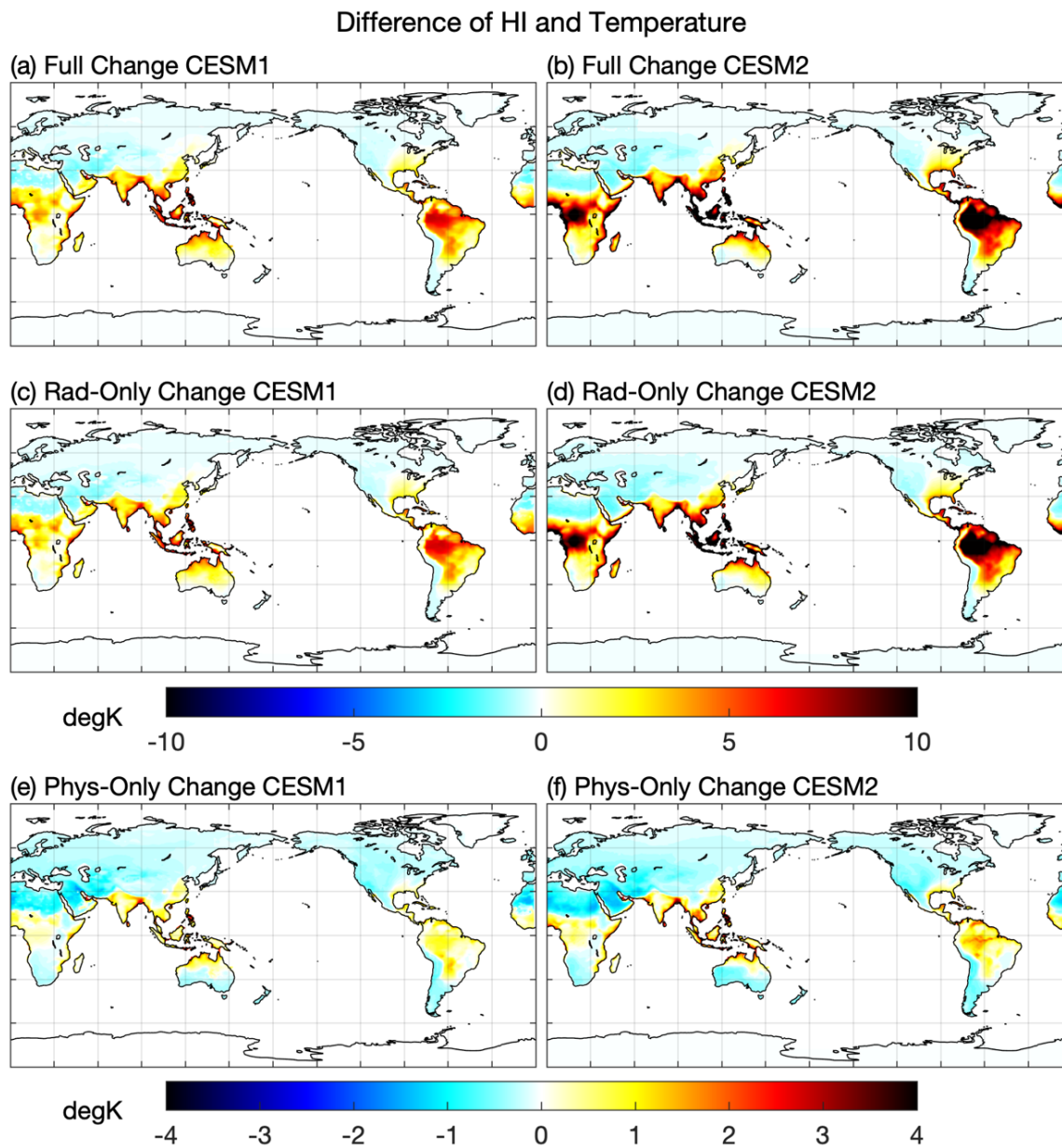


Figure 23: Difference Between the Mean Heat Index and Temperature Changes in the (a,b) Full (c,d) Radiation Only (e,f) Physiology Only Simulations. The higher color bar corresponds to plots (a-d) and the lower to (e & f).

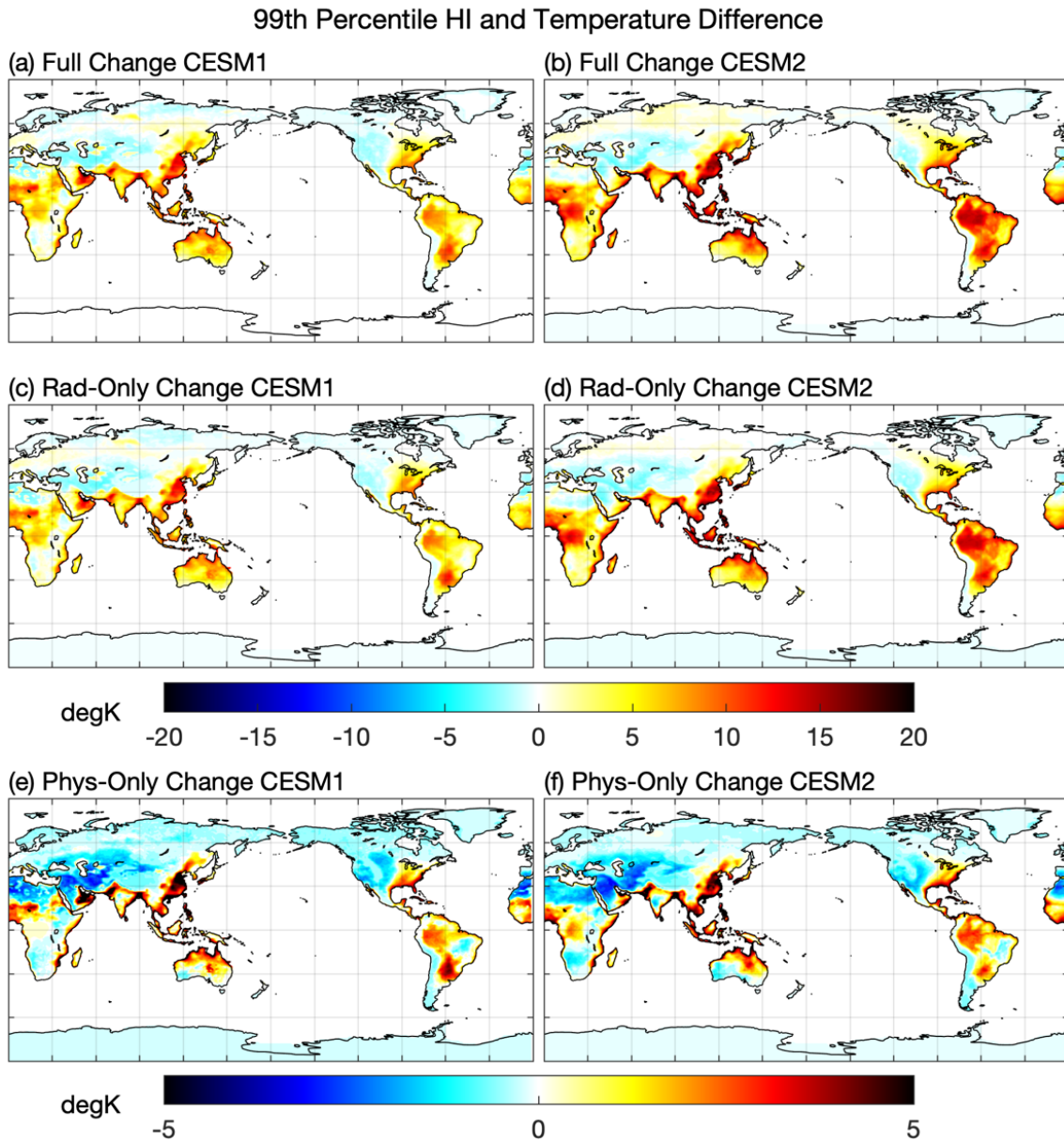


Figure 24: Difference Between the 99th Percentile Heat Index and Temperature Changes in the (a,b) Full (c,d) Radiation Only (e,f) Physiology Only Simulations. The higher color bar corresponds to plots (a-d) and the lower to (e & f).

Overall, the similarity between heat index and temperature increases due to plant-physiology implies that plant effects on temperature, as assessed by Skinner et al. (2018), may be the dominant influence compared to humidity changes. Since I postulated that plant-related impacts could increase temperature changes while simultaneously reducing humidity over land,

understanding which of these competing effects has a stronger influence on the heat index is a main question of this analysis. The magnitude of these differences can be seen in the difference between mean heat index and temperature change (Figure 22). Given the non-linear formation of the heat index equation and adjustments, regions in which the heat index change is slightly lower than temperature (teal colors) imply that increases in the heat index are mostly governed by temperature increases. In fact, temperature increases without a corresponding increase in specific humidity will lead to a lower relative humidity. In contrast, regions where the heat index change is substantially higher than temperature imply an important role of humidity changes. The differences between heat index and temperature largely separate the tropics and higher latitudes in all simulations, but tropical differences are particularly strong in the Full and Rad-only simulations. Phys-only values tend to be similar to Full and Rad-only outside the tropics (up to -1 degK), with smaller increases in the tropics. However, these results mask competing influences of temperature and specific humidity on relative humidity changes, which both change due to plant-physiology. Whether the temperature (denominator) or specific humidity (numerator) has a larger influence on the relative humidity contribution to the heat index changes is explored more below.

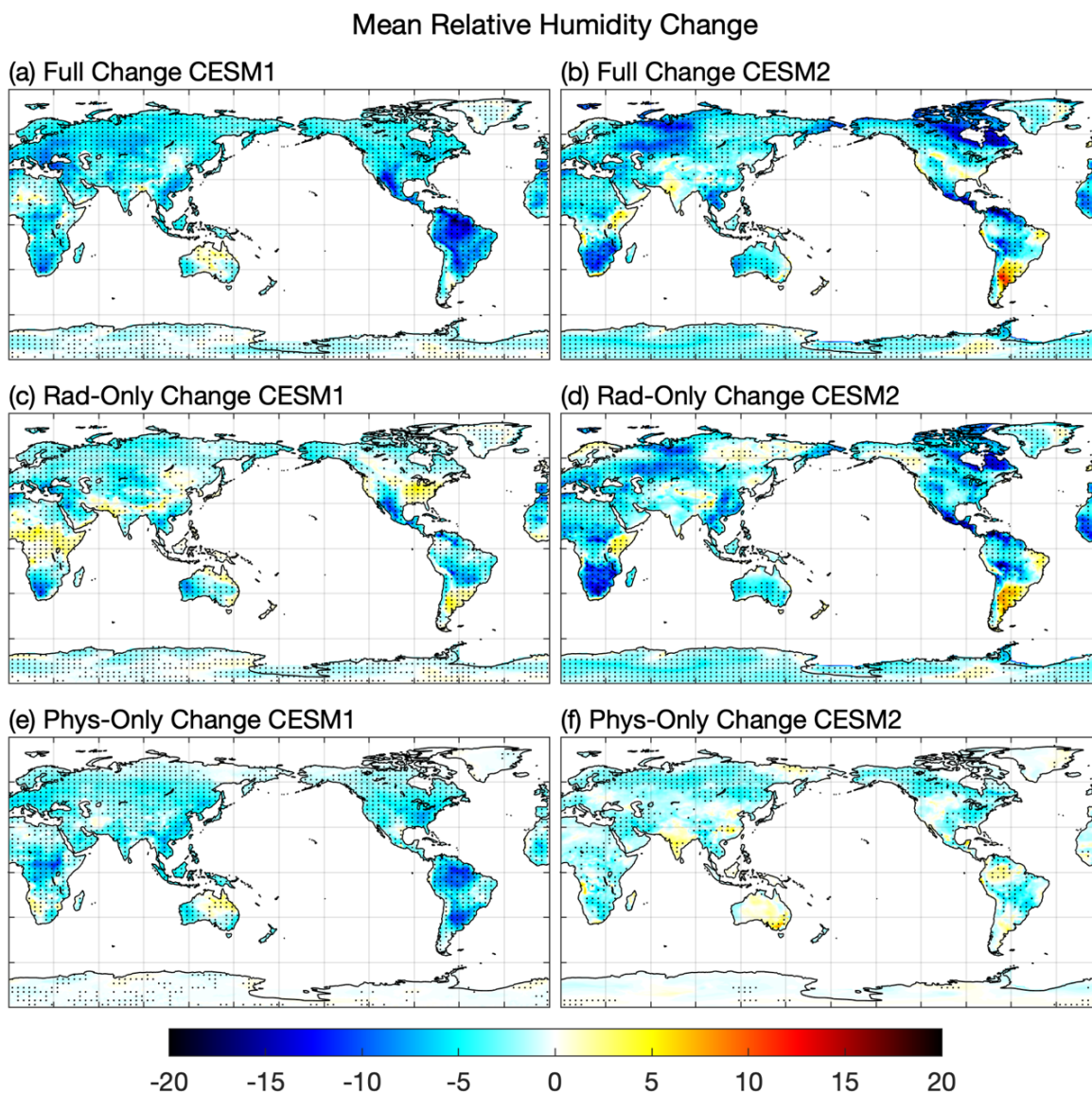


Figure 25: Changes of Mean Relative Humidity from the Pre-Industrial to the (a,b) Full (c,d) Radiation Only (e,f) Physiology Only Simulations. Stippling represents significance at the 95th percentile confidence interval. The higher color bar corresponds to plots (a-d) and the lower to (e & f). Stippling represents significance at the 95th percentile.

To understand what is causing the differences between heat index and temperature, we must look at the other component of HI, relative humidity (Figure 24), which shows a general reduction in all climates, with the exception of a few regions, in all simulations. As mentioned above, relative humidity changes are influenced by both specific humidity (Figure 25) and temperature (Figure 20) changes. By looking at the specific humidity change, it is clear that

reductions in relative humidity in the Full and Rad simulations must be driven primarily by increased temperature, rather than decreases in atmospheric moisture. Due to the nature of its calculation, as temperature increases, relative humidity will decrease, as the saturated moisture content is governed by the Clausius-Clapeyron relation. In the full and rad-only simulations, there is a significant increase of atmospheric moisture everywhere, but particularly across the tropics. This change is even more pronounced in CESM2, with increase of over 5g/kg over majority of the tropical regions. These areas of strong increase map nearly identically onto the regions with the strongest differences between HI and temperature (Figure 22). Interestingly, the magnitude of the Full relative humidity changes is similar in both model versions, despite much smaller magnitude changes due to Rad-only in CESM1. Both model versions have reductions in relative humidity due to plant-related process, but this effect is larger in CESM1, especially over tropical forest regions, and projects strongly onto the decreases seen in the Full simulation.

In contrast to what is seen in the full and rad-only simulations, specific humidity in the phys-only simulations have decreases over large portions of the globe. This is to be expected, as increasing CO₂ reduces stomatal conductance, which limits canopy transportation, reducing the amount of water lost from the plant to the surrounding air. The smaller regions experiencing increasing specific humidity in the phys-only runs are likely due to the competing effect of CO₂ enrichment on leaf area and/or precipitation changes. There are more regions with increases in CESM2, and overall the reductions are much weaker than CESM1, which may result from either a weaker stomatal conductance effect or stronger plant growth. The physiological processes that lead to this reduction of specific humidity, as well as how they are different between model versions, is explored in part 3.

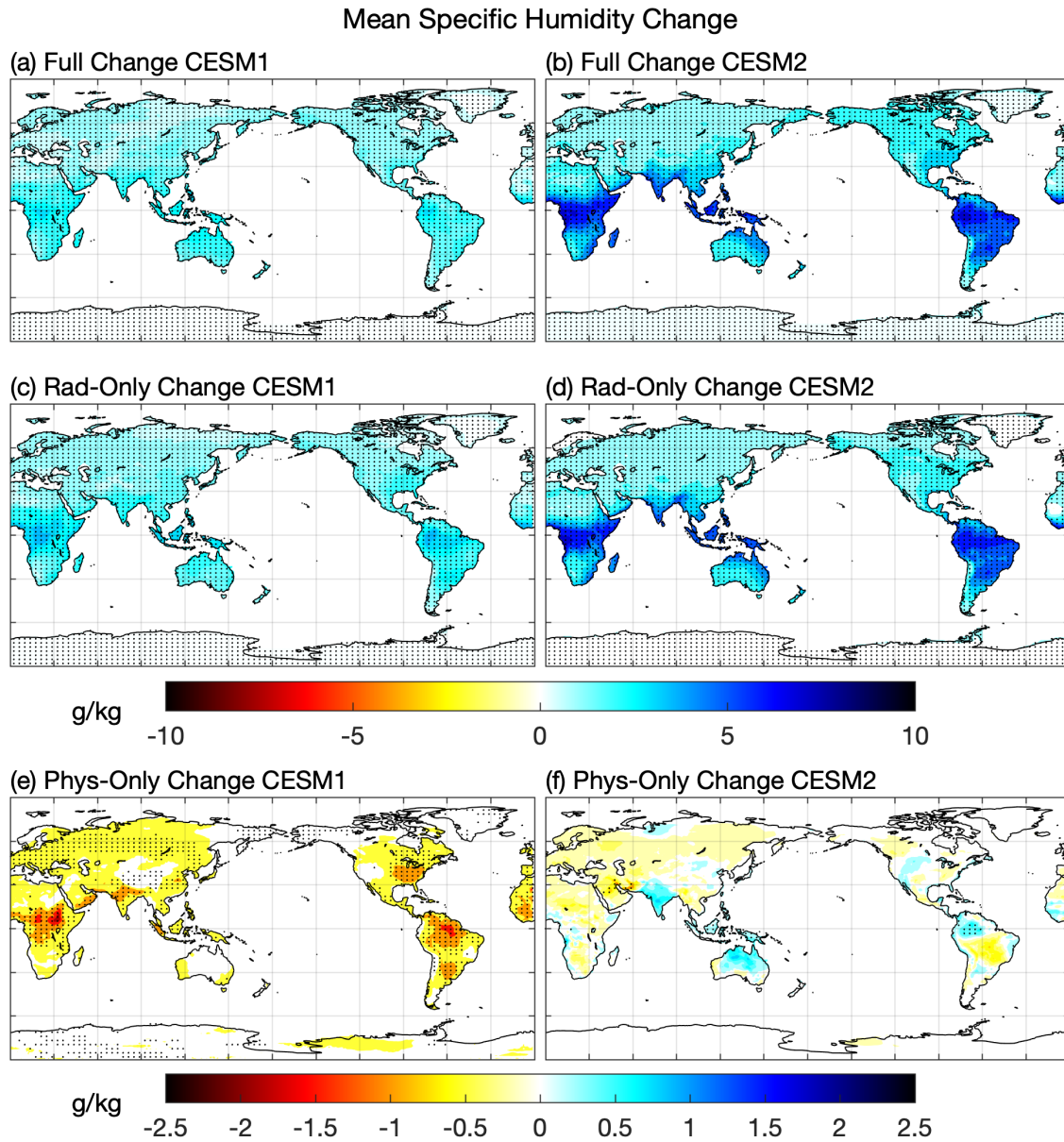


Figure 26: Changes of Mean Specific Humidity from the Pre-Industrial to the (a,b) Full (c,d) Radiation Only (e,f) Physiology Only Simulations. The higher color bar corresponds to plots (a-d) and the lower to (e & f). Stippling represents significance at the 95th percentile.

Overall, we can think about changes in the heat index resulting from changes in temperature and specific humidity, both of which also influence relative humidity. Radiative processes tend to increase both temperature and specific humidity, but the temperature changes have the dominant influence on relative humidity, which generally declines. Since temperature

tends to increase more at high latitudes, but only specific humidity increases more at low latitudes, the humidity contributions are what exert a stronger influence on the heat index change in the tropics due to radiation only. Plant-physiological processes also tend to increase temperature, but generally decrease specific humidity over most regions, both of which reduce relative humidity, particularly in CESM1. Since the heat index generally increases in response to plant CO₂ physiological forcing, it can be concluded that the influences on temperature are the dominant effect.

In summary, mean and extreme heat index values increase significantly in response to CO₂ radiative warming, particularly at high latitudes (due to temperature increases) and in the tropics (due to temperature and specific humidity increases). Plant-physiological responses to rising CO₂ also contribute to increases in the mean heat index over all land, but have a much stronger response in CESM1 than CESM2. Extreme heat index values generally also increase due to plant-physiology, but have some regions of little or negative changes. The most extreme warming occurs at high latitudes in the northern hemisphere in both model versions, and South America in CESM1. Increases in the heat index in Phys-only simulations are primarily driven by rising temperatures. This is offset slightly by decreases in relative humidity, particularly in CESM1, due to both higher temperatures and large reductions in specific humidity. Despite this offsetting effect, plant-physiology contributes to about 10-20% of the Full change in CESM1. Altogether, plants play a stronger role in influencing the Full climate changes in CESM1 than CESM2, with greater increases in the heat index and temperature and decreases in humidity. The underlying causes of these model differences are explored in part 3 below.

PART 3: Disentangling the competing influences of plant physiological forcing on heat and atmospheric moisture changes

In part 2, the results highlighted contributions of physiological forcing to changes in heat index, temperature, relative humidity, and specific humidity. The heat index and relative humidity are both functions of temperature and specific humidity, and the analysis demonstrated increases and decreases in these two variables, respectively, as a result of plant responses to rising CO₂. The results in part 2 also showed a much stronger response in CESM1 than CESM2 for all of these variables, which demonstrates the need to better constrain the extent to which plant processes can modulate climate changes. As a first step, this section begins to disentangle the different climatic drivers that plants contribute to these changes, namely through their influences on evaporation, which subsequently repartitions latent and sensible heating. The main driving force behind this assessment is the sensitivities to rising atmospheric CO₂ concentrations. As the concentration increases, the stomata on the leaves of plants may open less (i.e., reduced stomatal conductance), which reduces water lost through transpiration. Transpiration, in combination with ground and canopy evaporation, makes up the total evapotranspiration. Plants also respond to rising CO₂ through increases in photosynthesis and growth. If this growth occurs as an increase in leaf area, it may counter changes in stomatal conductance by increasing the number of stomata. It may also allow for more rainwater to be intercepted by the surfaces of leaves and increase canopy evaporation. The representation of these competing plant effects are explored in the following set of figures to determine their influences on the results of part 2.

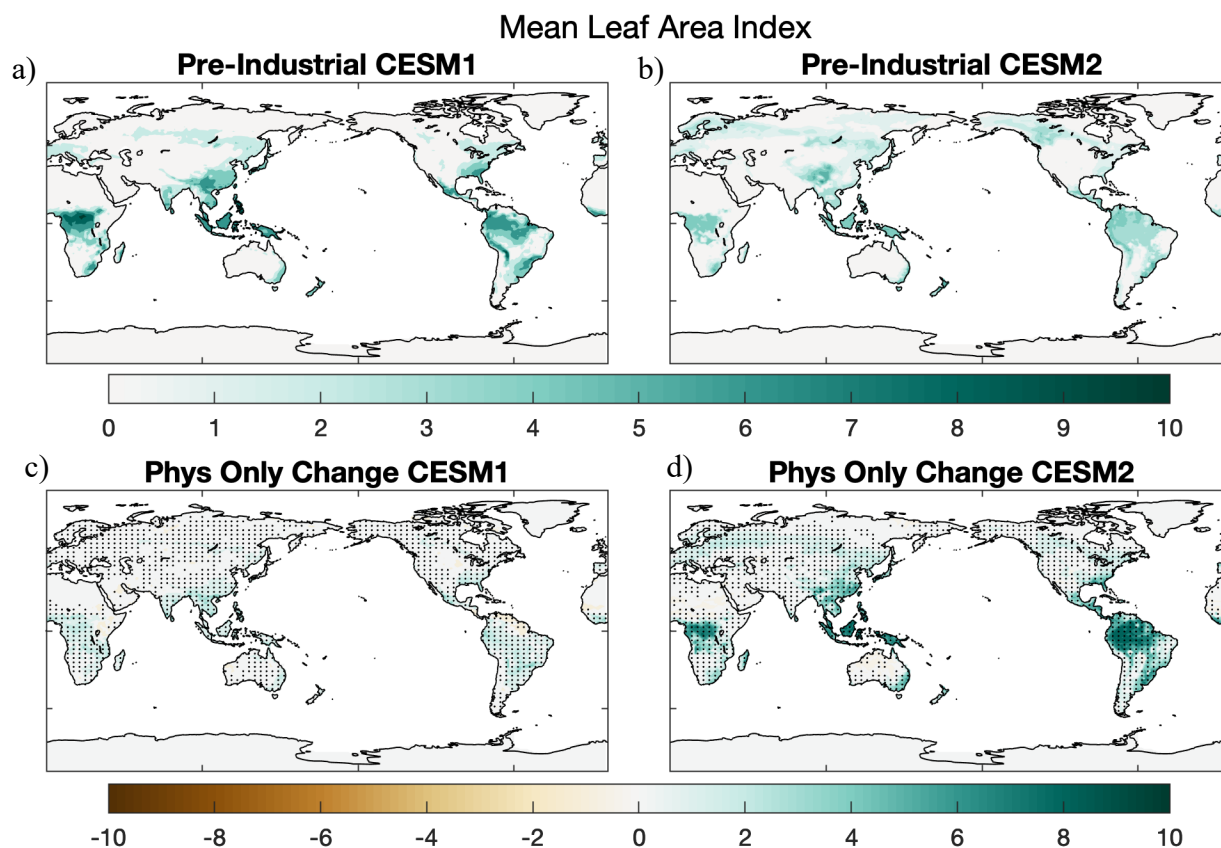


Figure 27: Mean Leaf Area Index in the Pre-Industrial Climate for (a) CESM1 and (b) CESM2. Change from Pre-Industrial to Physiology-Only Run in (c) CESM1 and (d) CESM2. Units: m^2/m^2 . Stippling represents significance at the 95th percentile.

To first understand how plant processes that drive evapotranspiration are changing, we must investigate how much they are growing. Leaf area index (LAI) is a measure of the amount of plant cover in a given unit area, so changes in this quantity can be used to signify growth as it relates to evapotranspiration. As seen in Figure 26, there is vastly more modeled increases in LAI in CESM2 than in CESM1 (bottom row). It should be noted that this metric only assesses leaf growth, not overall growth, and part of the difference may be related to the representation of carbon allocation to leaves relative to other parts of the plant. However, leaf allocation is most relevant to changes in evapotranspiration. Additionally, while plants appear to grow less in

CESM1, LAI values in the pre-industrial simulation are much greater than CESM2. This means there may be greater potential to increase LAI in response to rising CO₂. Together, these may contribute to greater rates of change in CESM2 with higher LAI-CO₂ sensitivity, which may have a variety of different impacts on evapotranspiration and its components. Larger increases in LAI would also imply a larger decrease in the surface albedo, but this appears to be a secondary effect given that temperature increases are larger in CESM1 than CESM2.

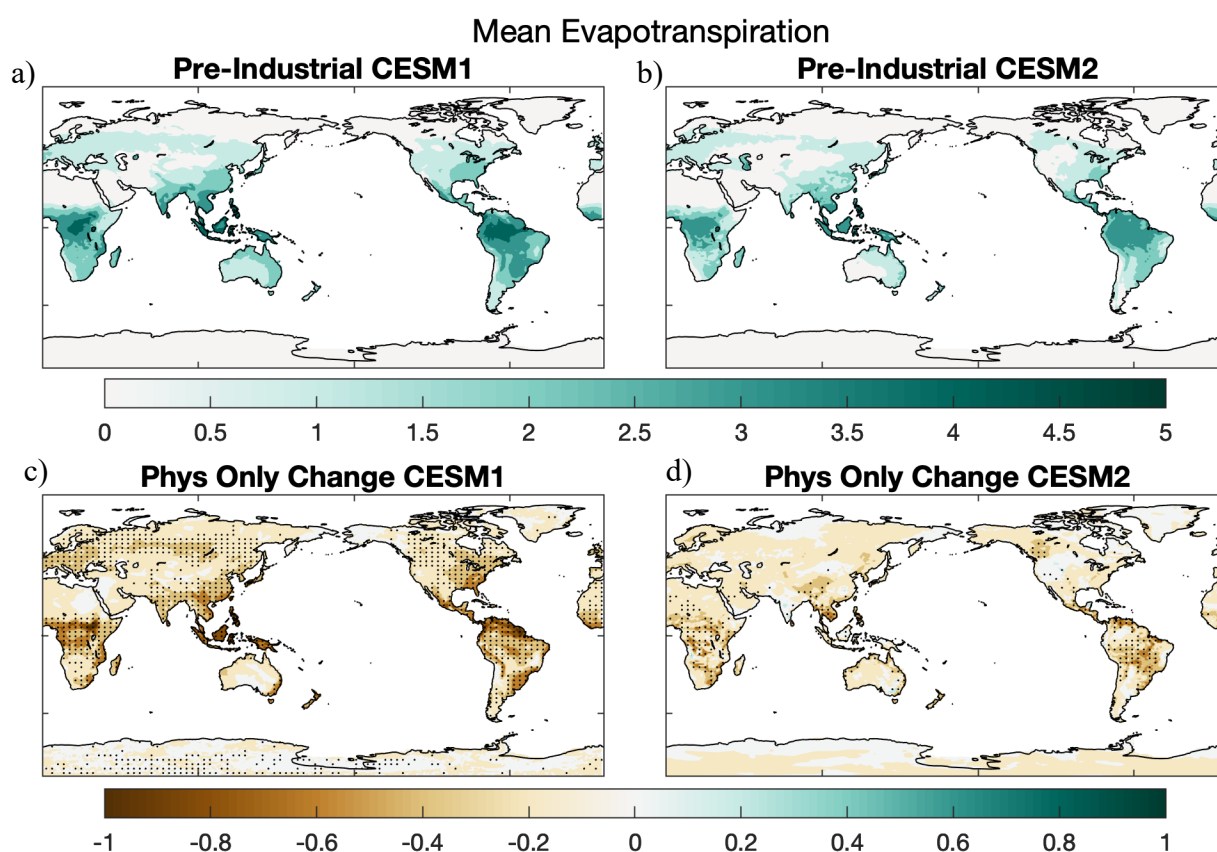


Figure 28: Mean Evapotranspiration in the Pre-Industrial Climate for (a) CESM1 and (b) CESM2. Change from Pre-Industrial to Physiology-Only Run in (c) CESM1 and (d) CESM2. Units: mm/day. Stippling represents significance at the 95th percentile.

Evapotranspiration is a combination of biological or physical process, including transpiration and evaporation from both the canopy and the ground surface. In both versions of CESM, there is an overall reduction of evapotranspiration (Figure 27). The highest magnitudes

of this decrease are located in the tropical forest regions, where there is the world's densest vegetation, but decreases are ubiquitous over all land, even high-latitudes. These reductions are much smaller in CESM2 than in CESM1. This may be in part due to slightly larger pre-industrial values in CESM1 allowing for the potential of a larger decline, but also differences in the sensitivities of stomatal conductance to increasing CO_2 and the influences of a larger LAI- CO_2 sensitivities in CESM2. These sensitivities are unfolded by breaking out the separate components of evapotranspiration below.

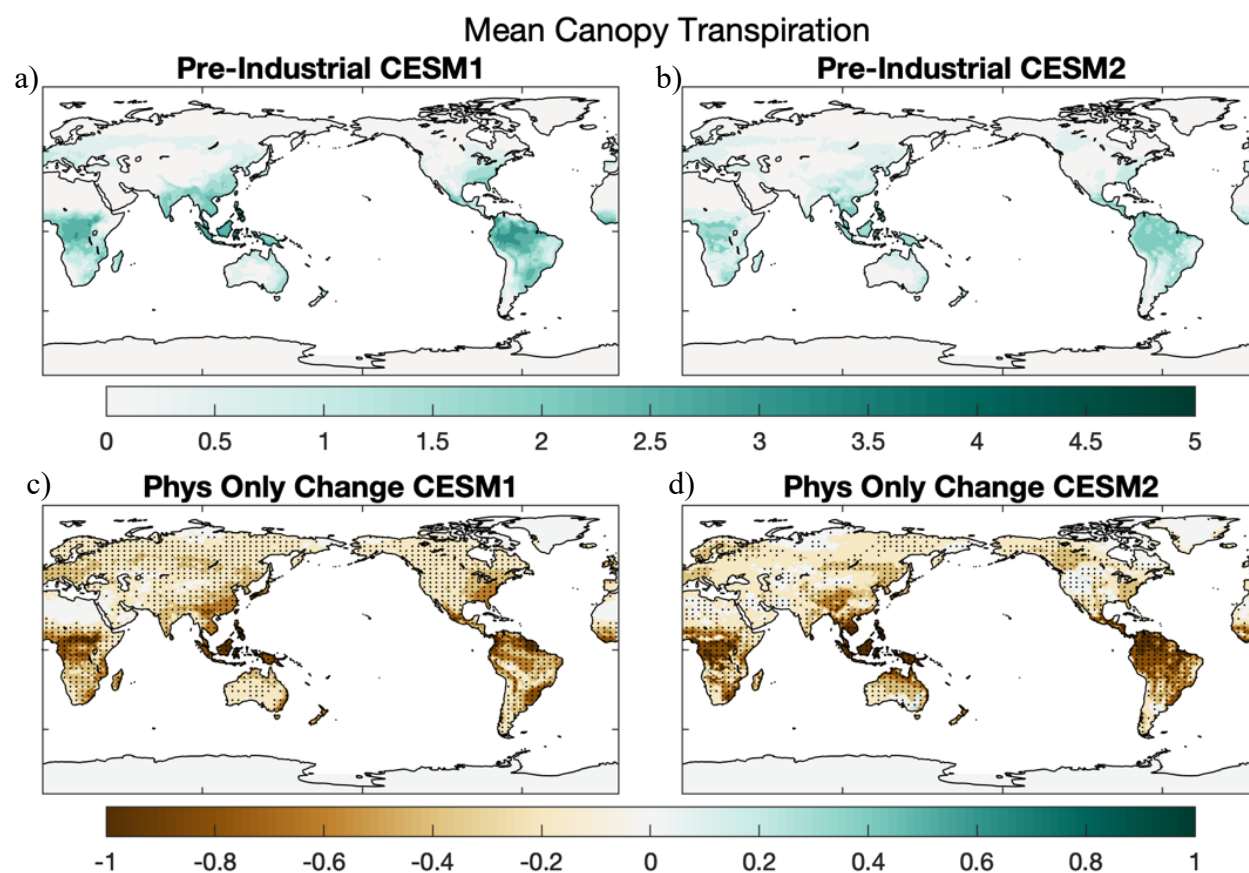


Figure 29: Mean Canopy Transpiration in the Pre-Industrial Climate for (a) CESM1 and (b) CESM2. Change from Pre-Industrial to Physiology-Only Run in (c) CESM1 and (d) CESM2. Units: mm/day. Stippling represents significance at the 95th percentile.

In both versions of CESM, there is an overall reduction of canopy transpiration (Figure 28). Some regions are seeing a decrease of up to 1 mm/day, which accounts for a 20% decrease

of rates seen in the pre-industrial simulations. The highest magnitudes of this decrease are again located in the tropical regions. Unlike the total evapotranspiration changes, there are larger declines in canopy transpiration for CESM2 than CESM1, though the differences are small. Higher levels of CO₂ mean the stomata on the plant open less, leading to reduced water lost to the atmosphere by transpiration. Even with more stomata associated with larger LAI increases in CESM2, the transpiration rates decline everywhere. Differences between CESM1 and CESM2 may be in part due to the update from the Ball-Berry (1987) to the Medlyn (2011) models of stomatal conductance, in addition to differences in precipitation and other processes affecting the overall water budget.

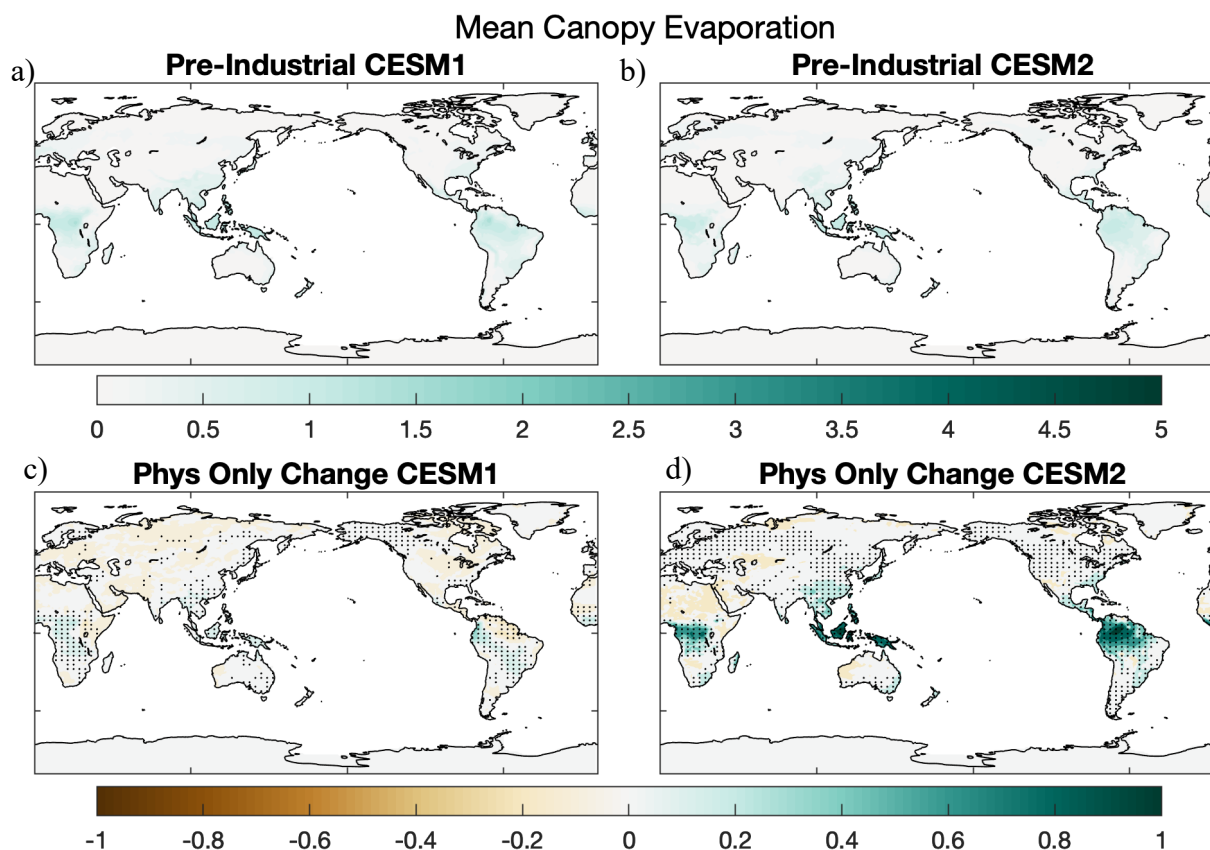


Figure 30: Mean Canopy Evaporation in the Pre-Industrial Climate for (a) CESM1 and (b) CESM2. Change from Pre-Industrial to Physiology-Only Run in (c) CESM1 and (d) CESM2. Units: mm/day. Stippling represents significance at the 95th percentile.

While the pre-industrial levels of canopy evaporation are nearly identical between the model versions, the changes resulting in the phys-only runs are vastly different (Figure 21). In CESM1, the canopy evaporation rate change is relatively low, with values in the range of ± 0.2 mm/day. This includes larger areas of small decreases across the northern high latitudes. CESM2 shows much greater change as areas in the tropics are projected to increase up to 1 mm/day or an increase of approximately 20% from pre-industrial levels. When there is a greater amount of leaf area, there is more surface area for rainwater to collect on and re-evaporate from. Since transpiration changes are relative similar between model versions, and ground evaporation changes are also similar and generally smaller (Figure 30), the contrast in canopy evaporation

changes is the main factor contributing to the difference in total evapotranspiration between CESM1 and CESM2 (Figure 27). These higher rates of canopy evaporation in CESM2 offset the reductions in transpiration, resulting in overall smaller decreases in evapotranspiration.

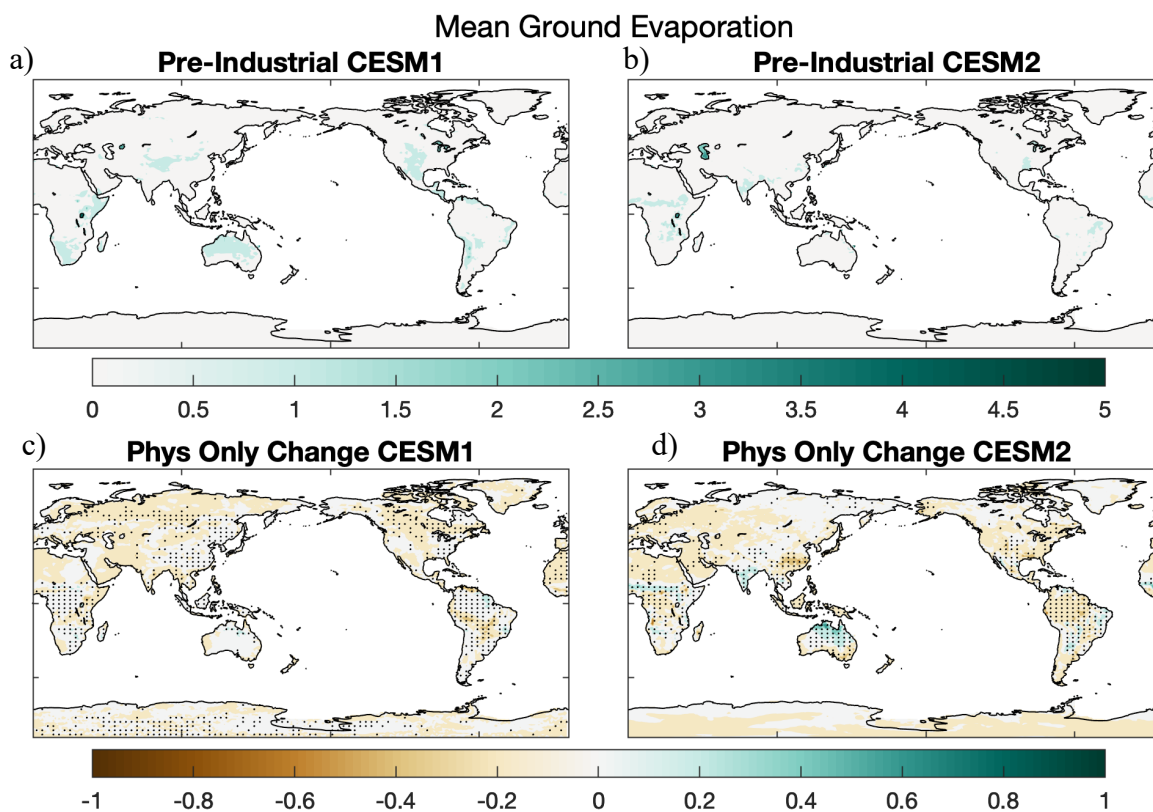


Figure 31: Mean Ground Evaporation in the Pre-Industrial Climate for (a) CESM1 and (b) CESM2. Change from Pre-Industrial to Physiology-Only Run in (c) CESM1 and (d) CESM2. Units: mm/hour. Stippling represents significance at the 95th percentile.

In summary, changes in evapotranspiration exert the main control on the temperature and humidity changes discussed in part 2. Reductions in evapotranspiration reduce a source of moisture to the overlying atmosphere, leading to lower specific humidity. Reductions in evapotranspiration also result in higher sensible heating and warming, contributing to increasing atmospheric temperature. The offsetting of transpiration by canopy evaporation means that the larger increases in LAI in CESM2 lead to smaller overall evapotranspiration changes, and thus

smaller impacts on the heat index. CESM2 has a strong stomatal conductance response and a strong LAI response, while CESM1 only has a strong stomatal conductance response. Without investigating these individual components, it might be concluded that plant responses are stronger in CESM1, while only assessing one or the other may lead to misleading conclusions. The results shown here highlight the importance of breaking out and better constraining the individual components of plant physiological processes in order to reduce uncertainties in their overall impacts on climate.

CHAPTER 5

DISCUSSION

The results of this study contain a number of key findings. The first of which concludes that hourly temperature and relative humidity output is not necessary for the calculation of the heat index at mean and 99th percentiles; but when using defined thresholds, it should at least be considered. The second findings show that around 2-3 degK of the projected increase of heat index is due to physiological forcing, with these numbers being more pronounced in CESM1 as compared to CESM2. For the 99th percentiles, there is a more sporadic warming pattern, with both increases and decreases of upwards to 4 degK. Majority of the increase comes from higher temperatures, with these regions seeing nearly identical patterns and magnitudes of warming. These results are consistent with Skinner et al., (2018) and Kala et. al., (2016), which found that CO₂ vegetation forcing is contributing to increases of heat wave days. Any of the increase in temperatures and/or the heat index in the physiology-only simulations is likely due to the reduction of atmospheric moisture, similar to the findings of Kirschbaum and McMillan (2018). This reduction of atmospheric moisture is in part to decreasing evapotranspiration rates. This effect is reduced in CESM2, because of the counteraction of reduced transpiration due to increased stomatal closure, and higher rates of canopy evaporation from greater leaf area. The difference between evapotranspiration rates in CESM1 and CESM2 is the rationale behind the differences in physiological warming. Despite these differences, physiological forcing is still playing a notable role in warming global temperatures.

CHAPTER 6

CONCLUSION

In this study, I investigated both the necessity of hourly temporal scale model output for calculating heat index; as well as the impact of plant physiological forcing on extreme heat, changes to atmospheric moisture, and how those combine to influence heat index. Previous research into the necessity of sub-daily scale found there to be statistically significant differences between averaging minimum and maximum temperature or taking a 24-hour average to get the average daily temperature (Bernhardt et al., 2018). In this study, I found there to be some significant differences, but not to the extent that this analysis could not be done with daily data. Future implications of these findings would include the confirmation that daily data is sufficient enough for the calculation of the heat index, so it is unnecessary for future model runs to output hourly temperature and relative humidity data.

Investigations into the impact of plant physiological forcing on heat index concluded that while majority of warming is coming from the increased greenhouse effect, plants are contributing a notable amount of warming in some regions, while cooling others. The main driving force behind these changes is the change in evapotranspiration rates. Transpiration acts to reduce the amount of water lost from the plant to the atmosphere, but there is the competing effect of canopy evaporation that increases water lost. Under models with higher canopy growth rates, evaporation will be greater, canceling out more of transpiration loss, leading to reduced evapotranspiration.

This analysis defined extreme heat as either 99th percentiles of temperature and heat index, or by the categories defined by the National Weather Service (NOAA, 2019). Motivation for future work includes investigations into heat wave events, such as those presented in (Perkins-Kirkpatrick & Lewis, 2020; Skinner et al., 2018; Smith et al., 2013) or one of the many other studies investigating heat waves. Additionally, I only investigated the heat index, one of many different heat stress metrics. Buzan et al., (2015) presents a number of these metrics, which factor in temperature, humidity, vapor pressure, mixing ratio, and/or wind speed. Future work should include an investigation into both heatwaves, and one or more of these metrics to better encapsulate the impact that physiological forcing is having on extreme heat events.

Overall, the contribution of both the greenhouse effect and physiological forcing is leading to increased global temperatures, and associated heat index. Without alterations to the current rate of greenhouse gas emissions, this extreme heat will only worsen, and the ramifications will become even more grave. According to the IPCC, global populations exposed to heat waves will continue to increase, along with heat-related mortality (IPCC, 2021). I hope the findings of this study will broaden the understanding of the role of plants impact on extreme heat, and that the findings will help inform policy decisions that can play a role in reducing the corresponding risks.

REFERENCES

- Alessi, M. J., & DeGaetano, A. T. (2020). Future extreme hourly wet bulb temperatures using downscaled climate model projections of temperature and relative humidity. *Theoretical and Applied Climatology*, 142(3–4), 1245–1254. <https://doi.org/10.1007/s00704-020-03368-0>
- Arias, P.A., N. Bellouin, E. Coppola, R.G. Jones, G. Krinner, J. Marotzke, V. Naik, M.D. Palmer, G.-K. Plattner, J. Rogelj, M. Rojas, J. Sillmann, T. Storelvmo, P.W. Thorne, B. Trewin, K. Achuta Rao, B. Adhikary, R.P. Allan, K. Armour, G. Bala, R. Barimalala, S. Berger, J.G. Canadell, C. Cassou, A. Cherchi, W. Collins, W.D. Collins, S.L. Connors, S. Corti, F. Cruz, F.J. Dentener, C. Dereczynski, A. Di Luca, A. Diongue Niang, F.J. Doblas-Reyes, A. Dosio, H. Douville, F. Engelbrecht, V. Eyring, E. Fischer, P. Forster, B. Fox-Kemper, J.S. Fuglestedt, J.C. Fyfe, N.P. Gillett, L. Goldfarb, I. Gorodetskaya, J.M. Gutierrez, R. Hamdi, E. Hawkins, H.T. Hewitt, P. Hope, A.S. Islam, C. Jones, D.S. Kaufman, R.E. Kopp, Y. Kosaka, J. Kossin, S. Krakovska, J.-Y. Lee, J. Li, T. Mauritsen, T.K. Maycock, M. Meinshausen, S.-K. Min, P.M.S. Monteiro, T. Ngo-Duc, F. Otto, I. Pinto, A. Pirani, K. Raghavan, R. Ranasinghe, A.C. Ruane, L. Ruiz, J.-B. Sallée, B.H. Samset, S. Sathyendranath, S.I. Seneviratne, A.A. Sörensson, S. Szopa, I. Takayabu, A.-M. Tréguier, B. van den Hurk, R. Vautard, K. von Schuckmann, S. Zaehle, X. Zhang, and K. Zickfeld, (2021): Technical Summary. In *Climate Change 2021: The Physical Science Basis. Contribution of Working Group I to the Sixth Assessment Report of the Intergovernmental Panel on Climate Change* [Masson-Delmotte, V., P. Zhai, A. Pirani, S.L. Connors, C. Péan, S. Berger, N. Caud, Y. Chen, L. Goldfarb, M.I. Gomis, M. Huang, K. Leitzell, E. Lonnoy, J.B.R. Matthews, T.K. Maycock, T. Waterfield, O. Yelekçi, R. Yu, and B. Zhou (eds.)]. Cambridge University Press, Cambridge, United Kingdom and New York, NY, USA, pp. 33–144, doi:10.1017/9781009157896.002.

- Bacmeister, J. T., Hannay, C., Medeiros, B., Gettelman, A., Neale, R., Fredriksen, H. B., Lipscomb, W. H., Simpson, I., Bailey, D. A., Holland, M., Lindsay, K., & Otto-Bliesner, B. (2020). CO2 Increase Experiments Using the CESM: Relationship to Climate Sensitivity and Comparison of CESM1 to CESM2. *Journal of Advances in Modeling Earth Systems*, *12*(11), 1–39. <https://doi.org/10.1029/2020MS002120>
- Alessi, M. J., & DeGaetano, A. T. (2020). Future extreme hourly wet bulb temperatures using downscaled climate model projections of temperature and relative humidity. *Theoretical and Applied Climatology*, *142*(3–4), 1245–1254. <https://doi.org/10.1007/s00704-020-03368-0>
- Arias, P. A., Bellouin, N., Coppola, E., Jones, R. G., Krinner, G., Marotzke, J., Naik, V., Palmer, M. D., Plattner, G.-K., Rogelj, J., Rojas, M., Sillmann, J., Storelvmo, T., Thorne, P. W., Trewin, B., Rao, K. A., Adhikary, B., Allan, R. P., Armour, K., ... Zickfeld, K. (2021). Foreword Technical and Preface. In *Climate Change and Land: an IPCC special report on climate change, desertification, land degradation, sustainable land management, food security, and greenhouse gas fluxes in terrestrial ecosystems*. <https://doi.org/10.1017/9781009157896.002>
- Bacmeister, J. T., Hannay, C., Medeiros, B., Gettelman, A., Neale, R., Fredriksen, H. B., Lipscomb, W. H., Simpson, I., Bailey, D. A., Holland, M., Lindsay, K., & Otto-Bliesner, B. (2020). CO2 Increase Experiments Using the CESM: Relationship to Climate Sensitivity and Comparison of CESM1 to CESM2. *Journal of Advances in Modeling Earth Systems*, *12*(11), 1–39. <https://doi.org/10.1029/2020MS002120>
- Ball, J. T., Wood, I. E., & Berry, J. A. (1987). A Model Predicting Stomatal Conductance and its Contribution to the Control of Photosynthesis Under Different Environmental Conditions. *Progress in Photosynthesis Research*, *IV*(1), 221–222.
- Bernhardt, J., Carleton, A. M., & LaMagna, C. (2018). A comparison of daily temperature-averaging methods: Spatial variability and recent change for the CONUS. *Journal of Climate*, *31*(3), 979–996. <https://doi.org/10.1175/JCLI-D-17-0089.1>

- Buzan, J. R., Oleson, K., & Huber, M. (2015). Implementation and comparison of a suite of heat stress metrics within the Community Land Model version 4.5. *Geoscientific Model Development*, 8(2), 151–170. <https://doi.org/10.5194/gmd-8-151-2015>
- Danabasoglu, G., Lamarque, J. F., Bacmeister, J., Bailey, D. A., DuVivier, A. K., Edwards, J., Emmons, L. K., Fasullo, J., Garcia, R., Gettelman, A., Hannay, C., Holland, M. M., Large, W. G., Lauritzen, P. H., Lawrence, D. M., Lenaerts, J. T. M., Lindsay, K., Lipscomb, W. H., Mills, M. J., ... Strand, W. G. (2020). The Community Earth System Model Version 2 (CESM2). *Journal of Advances in Modeling Earth Systems*, 12(2), 1–35. <https://doi.org/10.1029/2019MS001916>
- Grundstein, A. J., Hosokawa, Y., & Casa, D. J. (2018). Fatal Exertional Heat Stroke and American Football Players: The Need for Regional Heat-Safety Guidelines. *Journal of Athletic Training*, 53(1), 43–50. <https://doi.org/10.4085/1062-6050-445-16>
- Horton, R. M., Mankin, J. S., Lesk, C., Coffel, E., & Raymond, C. (2016). A Review of Recent Advances in Research on Extreme Heat Events. *Current Climate Change Reports*, 2(4), 242–259. <https://doi.org/10.1007/s40641-016-0042-x>
- Jones, C. D., Arora, V., Friedlingstein, P., Bopp, L., Brovkin, V., Dunne, J., Graven, H., Hoffman, F., Ilyina, T., John, J. G., Jung, M., Kawamiya, M., Koven, C., Pongratz, J., Raddatz, T., Randerson, J. T., & Zaehle, S. (2016). C4MIP-The Coupled Climate-Carbon Cycle Model Intercomparison Project: Experimental protocol for CMIP6. *Geoscientific Model Development*, 9(8), 2853–2880. <https://doi.org/10.5194/gmd-9-2853-2016>
- Kala, J., De Kauwe, M. G., Pitman, A. J., Medlyn, B. E., Wang, Y. P., Lorenz, R., & Perkins-Kirkpatrick, S. E. (2016). Impact of the representation of stomatal conductance on model projections of heatwave intensity. *Scientific Reports*, 6(January), 1–7. <https://doi.org/10.1038/srep23418>
- Lee, D., & Brenner, T. (2015). Perceived temperature in the course of climate change: An analysis of global heat index from 1979 to 2013. *Earth System Science Data*, 7(2), 193–202. <https://doi.org/10.5194/essd-7-193-2015>
- Lindsay, K., Bonan, G. B., Doney, S. C., Hoffman, F. M., Lawrence, D. M., Long, M. C., Mahowald, N. M., Moore, J. K., Randerson, J. T., & Thornton, P. E. (2014). Preindustrial-

- control and twentieth-century carbon cycle experiments with the Earth system model CESM1(BGC). *Journal of Climate*, 27(24), 8981–9005. <https://doi.org/10.1175/JCLI-D-12-00565.1>
- Lorenz, R., Stalhandske, Z., & Fischer, E. M. (2019). Detection of a Climate Change Signal in Extreme Heat, Heat Stress, and Cold in Europe From Observations. *Geophysical Research Letters*, 46(14), 8363–8374. <https://doi.org/10.1029/2019GL082062>
- Medlyn, B. E., Duursma, R. A., Eamus, D., Ellsworth, D. S., Prentice, I. C., Barton, C. V. M., Crous, K. Y., De Angelis, P., Freeman, M., & Wingate, L. (2011). Reconciling the optimal and empirical approaches to modelling stomatal conductance. *Global Change Biology*, 17(6), 2134–2144. <https://doi.org/10.1111/j.1365-2486.2010.02375.x>
- Rothfusz, L. P. (1990). The heat index equation (or, more than you ever wanted to know about heat index). *Fort Worth, Texas: National Oceanic and Atmospheric Administration, National Weather Service, Office of Meteorology*, 23–90. <papers://c6bd9143-3623-4d4f-963f-62942ed32f11/Paper/p395>
- Segnalini, M., Bernabucci, U., Vitali, A., Nardone, A., & Lacetera, N. (2013). Temperature humidity index scenarios in the Mediterranean basin. *International Journal of Biometeorology*, 57(3), 451–458. <https://doi.org/10.1007/s00484-012-0571-5>
- Smith, T. T., Zaitchik, B. F., & Gohlke, J. M. (2013). Heat waves in the United States: Definitions, patterns and trends. *Climatic Change*, 118(3–4), 811–825. <https://doi.org/10.1007/s10584-012-0659-2>
- Steadman, R. G. (1979). The Assessment of Sultriness. Part I: A Temperature-Humidity Index Based on Human Physiology and Clothing Science. *Journal of Applied Meteorology*, 18(7), 861–873. [https://doi.org/10.1175/1520-0450\(1979\)018<0861:TAOSPI>2.0.CO;2](https://doi.org/10.1175/1520-0450(1979)018<0861:TAOSPI>2.0.CO;2)
- Swann, A. L. S., F. M. Hoffman, C. D. Koven and J. T. Randerson (2016), Plant responses to increasing CO2 reduce estimates of climate impacts on drought severity, *Proc. Natl. Acad. Sci. U.S.A.*, 113(36), 10019-10024. <https://doi.org/10.1073/pnas.1604581113>

- Taylor, K. E., Stouffer, R. J., & Meehl, G. A. (2012). An overview of CMIP5 and the experiment design. *Bulletin of the American Meteorological Society*, 93(4), 485–498.
<https://doi.org/10.1175/BAMS-D-11-00094.1>
- Ukkola, A. M., Pitman, A. J., Donat, M. G., De Kauwe, M. G., & Angéilil, O. (2018). Evaluating the Contribution of Land-Atmosphere Coupling to Heat Extremes in CMIP5 Models. *Geophysical Research Letters*, 45(17), 9003–9012. <https://doi.org/10.1029/2018GL079102>
- Vicedo-Cabrera, A. M., Scovronick, N., Sera, F., Royé, D., Schneider, R., Tobias, A., Astrom, C., Guo, Y., Honda, Y., Hondula, D. M., Abrutzky, R., Tong, S., Coelho, M. de S. Z. S., Saldiva, P. H. N., Lavigne, E., Correa, P. M., Ortega, N. V., Kan, H., Osorio, S., ... Gasparrini, A. (2021). The burden of heat-related mortality attributable to recent human-induced climate change. *Nature Climate Change*, 11(6), 492–500.
<https://doi.org/10.1038/s41558-021-01058-x>
- Walker, A. P., et al. (2014), Comprehensive ecosystem model-data synthesis using multiple data sets at two temperate forest free-air CO₂ enrichment experiments: Model performance at ambient CO₂ concentration, *J. Geophys. Res. Biogeosci.*, 119, 937–964,
<https://doi.org/10.1002/2013JG002553>
- WHO. (2018, June 1). Heat and health. Retrieved April 06, 2021, from
<https://www.who.int/news-room/fact-sheets/detail/climate-change-heat-and-health>
- Zhao, Q., Guo, Y., Ye, T., Gasparrini, A., Tong, S., Overcenco, A., Urban, A., Schneider, A., Entezari, A., Vicedo-Cabrera, A. M., Zanobetti, A., Analitis, A., Zeka, A., Tobias, A., Nunes, B., Alahmad, B., Armstrong, B., Forsberg, B., Pan, S. C., ... Li, S. (2021). Global, regional, and national burden of mortality associated with non-optimal ambient temperatures from 2000 to 2019: a three-stage modelling study. *The Lancet Planetary Health*, 5(7), e415–e425. [https://doi.org/10.1016/S2542-5196\(21\)00081-4](https://doi.org/10.1016/S2542-5196(21)00081-4)